Solar radio bursts and low frequency radio emissions from space

Rico Behlke

IRF Scientific Report 275
2001

ISSN 0284-1703

INSTITUTET FÖR RYMDFYSIK
SWEDISH INSTITUTE OF SPACE PHYSICS

Solar radio bursts and low frequency radio emissions from space

Diploma Thesis
by

Rico Behlke
Swedish Institute of Space Physics
Uppsala division
SE-755 91 Uppsala, Sweden

IRF Scientific Report 275
2001

Abstract

This diploma work deals mainly with solar radio bursts. I motivate the study of these phenomena and give a historical overview of them. I also summarize radiative definitions and present plasma radiation emission processes. In particular, an overview of solar radio bursts is given. Furthermore, other planetary radio emissions on the example of Jupiter are reviewed and the importance of radio astronomy from space is pointed out. As detailed examples, solar type II and III bursts are described. Special emphasis is put on the initiating agents such as flares and coronal mass ejections, acceleration and emission processes. Finally, the possibilities of low frequency radio astronomy from space are presented on the example of the ALFA and Nanny missions.

Contents

List of Figures

List of Tables

1 Introduction

Scientific studies of radio signals of extraterrestrial origin, received on the ground, have a rather short history and include such developments as radio astronomy and the active probing of Earth's ionosphere. To the latter category belongs the Stimulated Electromagnetic Emission (SEE) technique discovered and developed at the Wave Group at the Uppsala Division of the Swedish Institute of Space Physics.

A future development of particular interest are space-borne observations of astrophysical low-frequency radio emissions which are not possible to observe on Earth due to the ionospheric shielding. Another development is the study, in-situ, of the EM generating mechanism associated with the ionospheric plasma turbulence induced in a systematic and controlled way. In fact, the two lines of development are closely related as several of the SEE mechanisms are similar to those occurring in the perturbed solar corona where solar radio bursts have their origin.

1.1 Why study solar radio bursts?

The research on solar radio bursts provides in many ways considerable possibilities for the study of important phenomena in solar physics. Firstly, these bursts are an ideal instrument for investigating acceleration processes which are responsible for the high exciter velocities, see Chapter 4.1. Secondly, solar radio bursts can be used as natural plasma probes traversing the corona and the interplanetary space, thus providing information about various space plasma parameters. Thirdly, plasma radiation processes may provide insight into different wave-particle and wave-wave interactions, see Chapter 4.2.

Let me quote J.P. Wild (1974):

> I have the feeling that to most astronomers the Sun is rather a nuisance. The reasons are quite complex. In the first place the Sun at once halves the astronomer's observing time from 24 to 12 hours, and then during most of the rest of the time it continues its perversity by illuminating the moon. Furthermore I have met numerous astronomers who regard solar astronomy to be now, as always before, in a permanent decline — rather like Vienesse music or English cricket. Nevertheless those who study the Sun and its planetary system occasionally make significant contributions. There were, for instance, Galileo and Newton who gave us mechanics and gravitation; Fraunhofer who gave us atomic spectra; Eddington and Bethe who pointed the way to nuclear energy; and Alfvén who gave us magneto-hydrodynamics. Perhaps the point to be recognized is that the Sun has more immediately to offer to physics rather than to astronomy.[1]

[1] See Contopoulos [31, pg. 3].

1.2 Historical review of solar radiation

Sir Oliver Lodge can be considered the person who made the first attempt to measure extraterrestrial radio emissions. In a lecture held on June 1, 1894, he states:

> I hope to try for long-wave radiation from the Sun, filtering out the ordinary well-known waves by a blackboard or other sufficient opaque substances.[2]

In a later edition of his lecture he admits that he failed getting any hints of solar radiation and blamed it on the artificial disturbances. But only more than forty years later the waves that Lodge had in mind were observed.

In 1932 Jansky [56] was the first to observe radio emissions of extraterrestrial origin. While performing studies of atmospheric statics he discovered a weak hissing static whose origin was unknown, but was connected to the rotation of the Earth. Jansky managed to deduce a number of interesting conclusions, for example a disk-like contribution of the radio sources around the Earth, which was confirmed later on.

After Jansky's outstanding discovery, many unpublished observations and attempts were made, but no exact location of the extraterrestrial radiation was asserted. Researchers such as Arakawa [4], Heightman [48] and Nakagami & Miya [84] studied these disturbances without understanding what they were observing.

The first detection of solar radio emission and the interpretation as such took place in 1942. In 1946 Hey [49] reported that metric solar radiation had been observed by British army equipment on February 27 and 28, 1942. No precise measurements were made but it was estimated that the intensity was 10^5 times higher than expected for blackbody radiation at a temperature of 6000 K. Furthermore, this event was associated with a flare that was visible on the Sun on February 28, 1942 [86]. Nearly at the same time, Southworth [96] received radio emission of the "quiet" Sun at centimetric wavelengths. The Second World War caused the publication of the results to be delayed which led to the fact that Reber [91] rediscovered metric solar radiation in 1943. He was the first to publish results on solar radiation, although he wrote only a few lines on the solar radiation itself in his report on galactic radiation. Besides that, his article gives an interesting insight in the observation equipment used at the time. In 1946 Hey et al. [51] published a second paper on the observation of subsidiary maxima at $\lambda = 5$ m already observed by Reber. Their assumption that the received radiation originated from discrete sources and not from the interstellar medium was later established by Bolton & Stanley [18] which can be considered as quite an important discovery.

Other observational highlights were the first measurement of thermal radio emission of the moon by Dicke & Beringer [36] in 1945 while actually observing thermal microwaves from atmospheric oxygen and water vapor. One of the

[2] See Lodge [71].

most outstanding discoveries was subsequently made by Ewen & Purcell [41] at Harvard University when, in 1951, they detected the 21 cm line radiation (1421 MHz) from the hyperfine splitting of the ground state of atomic hydrogen. Four years later Burke & Franklin [21] discovered Jupiter as a planetary radio source.

For a deeper insight into the history of radio astronomy I suggest the publications of Carpenter [28], which contains substantial bibliographies, Haddock [45], Hey [50] and Southworth [97].

Concerning the history of solar radio bursts, on which I put the main emphasis in this thesis, I refer to Chapter 3 on page 17.

2 Thermal plasma radiation

In this Chapter I give an overview of radiation definitions including different equilibrium models. Furthermore, plasma emission processes such as bremsstrahlung, gyromagnetic radiation and Čerenkov radiation are described.

2.1 Radiative definitions

When radiation with intensity I_ν at a given frequency ν passes through a medium, a certain amount of it will be absorbed or scattered and some amount will be added. If we let A denote the cross section area of the medium which the radiation beam encounters under normal angle θ, then, after a passage of a distance ds under a time interval dt, the absorbed or scattered part of the radiation is

$$dE_\nu^- = \alpha_\nu \, I_\nu \, dA \, ds \, dt \, d\nu \, d\Omega \tag{1}$$

and the radiation amount added is

$$dE_\nu^+ = j_\nu \, dA \, ds \, dt \, d\nu \, d\Omega, \tag{2}$$

where α_ν is the *(linear) extinction coefficient* and j_ν the *emission coefficient.* One can rewrite α_ν such that

$$\alpha_\nu = \sigma_\nu n = \kappa_\nu \rho, \tag{3}$$

where

1. σ_ν the *extinction coefficient* or cross-section per particle and n the absorber density
2. κ_ν the *mass extinction coefficient* or cross-section per unit mass and ρ the mass density.

With respect to stellar atmospheres κ_ν is often called *opacity.*

We now can define

1. The intensity
$$I_\nu = \frac{dE_\nu}{\cos\theta \; dA \; dt \; d\nu \; d\Omega} \tag{4}$$
2. the mean intensity
$$J_\nu = \frac{\int I_\nu \; d\Omega}{\int d\Omega} = \frac{1}{4\pi} \int I_\nu \; d\Omega \tag{5}$$
3. the flux
$$F_\nu = \int I_\nu \; \cos\theta \; d\Omega. \tag{6}$$

Making use of Eqs. (1) and (2) one obtains

$$dI_\nu = I_\nu(s+ds) - I_\nu(s) = j_\nu ds - \alpha_\nu I_\nu ds. \tag{7}$$

Let us now introduce the *source function*

$$S_\nu = \frac{j_\nu}{\alpha_\nu}, \tag{8}$$

the *optical depth*

$$d\tau_\nu = \alpha_\nu ds \tag{9}$$

and

$$\mu = \cos\theta \Rightarrow ds = \frac{dz}{\cos\theta} = \frac{dz}{\mu}. \tag{10}$$

By using these definitions one can rewrite Eq. (7) as

$$\mu \frac{dI_\nu}{d\tau_\nu} = -I_\nu + S_\nu. \tag{11}$$

This is the *radiation transfer equation* which one needs to solve. This form of Eq. (11) is only valid for so-called plane-parallel media, i.e.,

$$\frac{\Delta R}{R} \approx 0, \tag{12}$$

where R is the radius of the medium. The general expression for Eq. (11) is

$$\frac{\partial I_\nu}{\partial r}\frac{\cos\theta}{\kappa_\nu \rho} - \frac{\partial I_\nu}{\partial \theta}\frac{\sin\theta}{\kappa_\nu \rho\, r} = -I_\nu + S_\nu \tag{13}$$

which can be easily transformed into Eq. (11) assuming that θ does not depend on z.

The problem that occurs if one wants to solve Eq. (11) is the complexity of the source function S_ν. The ideal case is the *thermodynamic equilibrium* (TE) which is characterized by the equilibrium between all processes with their inverse processes and the equilibrium between matter and radiation, i.e., one needs only one temperature T to describe the plasma. Thus, the electromagnetic radiation of a plasma I_ν is isotropic (which implies $F_\nu \equiv 0$) and can be described by the radiation distribution of a black body or the *Planck function* B_ν:

$$B_\nu(T) = \frac{2h\nu^3}{c^2}\frac{1}{e^{(h\nu)/(kT)} - 1} \equiv I_\nu(T) \equiv S_\nu(T), \tag{14}$$

where h is the Planck constant and k the Boltzmann constant.

Other important quantities characterizing a plasma in thermodynamic equilibrium are the *Maxwellian velocity distribution*

$$n(v) = \frac{4}{\sqrt{\pi}} v^2 \left(\frac{m}{2kT}\right)^{3/2} e^{-(mv^2)/(2kT)} \tag{15}$$

and the *Boltzmann distribution* which gives the excitation population

$$\frac{n_j}{n} = \frac{g_j}{g_i} e^{E_{\rm ex}/(kT)}, \tag{16}$$

where n_j is the number of particles in the excited state j, n the total number of particles, g_j and g_i the statistical weight of the excited and ground state, respectively, and $E_{\rm ex}$ the excitation energy of state j. The *Saha equation* describes the ionization population

$$\frac{N_{r+1}}{N_r} = \frac{2}{N_e} \frac{U_{r+1}}{U_r} \left(\frac{2\pi m_{\rm e} kT}{h^2} \right)^{3/2} e^{E_{\rm ion}/(kT)}, \tag{17}$$

where N is the number of particles in state r and $r+1$, respectively, N_e the number of electrons, U the partition function and $E_{\rm ion}$ the ionization energy. The *ionization ratio* is the number of ions with nuclear charge Z in a plasma with at least r times ionized particles and is given by

$$x_r = \frac{\sum_{i=r}^{Z} n_i}{\sum_{i=0}^{Z} n_i} \leq 1. \tag{18}$$

Weakly ionized plasmas are characterized by $x_1 \ll 1$ and strongly ionized plasmas by $x_1 \approx 1$.

However, thermodynamic equilibrium is only valid for isotropic and isothermal media which are relatively uncommon in physics. A solution to this problem is the assumption of *local thermodynamic equilibrium* (LTE): While matter still can be considered to be in equilibrium with the local kinetic temperature, radiation deviates slightly from that temperature. Thus, one needs two quantities to describe to plasma: $T_{\rm matter}$ and $T_{\rm radiation}$. Since the radiation is no longer isotropic, the intensity is no longer given by the Planck function, and hence $I_\nu \neq B_\nu$. On the other hand $S_\nu = B_\nu$ still holds. In other words, LTE is valid if collisions dominate the energy partitioning of the matter more strictly than for the radiation, i.e., if $\epsilon_\nu \simeq 1$, where ϵ_ν is the destruction probability of the photon, defined by Eq. (25). In stellar interiors for example, we can assume LTE. Since $F_\nu \neq 0$, we do not encounter TE, but due to the high density there is a high collision rate and thus $\epsilon_\nu \simeq 1$.

What happens if one no longer can expect the Boltzmann equation (16) and the Saha equation (17) to hold? This is the case in *statistical equilibrium* (SE), i.e., each level of each element can be considered as steady state. Then one has to solve the rate equations for all populations, assuming steady states:

$$\begin{aligned} \frac{dn_i}{dt} = 0 &= \sum_{j \neq i} (n_j P_{ji} - n_i P_{ij}) \\ &= \sum_{j \neq i} n_j P_{ji} - n_i \sum_{j \neq i} P_{ij}, \end{aligned} \tag{19}$$

where

$$P_{ij} = A_{ij} + B_{ij} J_\nu + C_{ij}. \tag{20}$$

A_{ij}, B_{ij} and C_{ij} are the well-known Einstein coefficients [42]

$$\frac{A_{ij}}{B_{ij}} = \frac{2h\nu^3}{c^2} \tag{21}$$

$$\frac{B_{ij}}{B_{ji}} = \frac{g_j}{g_i} \tag{22}$$

$$\frac{C_{ij}}{C_{ji}} = \frac{g_j}{g_i} e^{(E_{ji})/(kT)}. \tag{23}$$

The problem which appears is that the rate equations (19) contain J_ν which one obtains from the radiation transfer equation (11). But to solve this, one needs $S_\nu = j_\nu/\kappa_\nu$ which depends on the populations, i.e., the number of absorbing and emitting particles. Thus, Eqs. (11) and (19) have to be solved together in a self-consistent manner, because any transition depends on all other transitions.

The most realistic case is of course by definition *non-local thermodynamic equilibrium* (NLTE). Under such conditions the source function contains a scattering term besides the thermal term expressed by B_ν:

$$S_\nu = \epsilon_\nu B_\nu + (1 - \epsilon_\nu) J_\nu, \tag{24}$$

where ϵ_ν is the destruction probability for the photon

$$\epsilon_\nu = \frac{C_{ij}}{A_{ij} + B_{ij} J_\nu + C_{ij}}. \tag{25}$$

Note that Eq. (25) holds only for two-level atoms. The term $(\epsilon_\nu B_\nu)$ describes the transformation of the energy of the destructed photon into thermal energy. On the other hand, the term $(1-\epsilon_\nu)$ is the scattering probability of the photon, i.e., no thermal energy is added. Thus, if there is a high scattering rate, i.e., $\epsilon_\nu \ll 1$, S_ν may differ quite a lot from B_ν.

After this overview over several equilibrium models let us take a look at the radiation transfer equation (11) itself. After multiplying it with an integrating factor e^τ one obtains

$$\frac{dI_\nu}{d\tau} e^\tau + I_\nu e^\tau = \frac{d}{d\tau} I_\nu e^\tau = S_\nu e^\tau. \tag{26}$$

Integration leads to

$$I_\nu e^\tau - I_{\nu o} = \int_0^\tau S_\nu \; e^\tau \; d\tau. \tag{27}$$

In a homogeneous medium of thickness D where S_ν does not change with location, Eq. (27) simplifies to

$$I_\nu(D) = I_\nu(0) e^{-\tau} + S_\nu (1 - e^{-\tau}). \tag{28}$$

Thus, for a optically thin medium, i.e., $\tau_\nu < 1$

$$I_\nu(D) \approx S_\nu \tag{29}$$

and for a optically thick medium, i.e., $\tau_\nu > 1$

$$I_\nu(D) \approx I_\nu(0) + [S_\nu - I_\nu(0)]\,\tau_\nu. \tag{30}$$

Let us pay attention to the two cases for $\tau_\nu > 1$:

1. $I_\nu(0) > S_\nu$: This leads to $S_\nu - I_\nu(0) < 0$ and thus an absorption line.
2. $I_\nu(0) < S_\nu$: One obtains $S_\nu - I_\nu(0) > 0$ and hence an emission line.

Because I just gave a rough overview, I suggest the following books for deeper understanding of this chapter: Böhm-Vitense [17] can be seen as an easy reading textbook, while Gray [42] gives a well-rounded view on the subject. Mihalas [81] in the end contains more sophisticated mathematical handwork for the understanding of radiation transfer.

2.2 Bremsstrahlung

Bremsstrahlung is emission caused by Coulomb interactions between charged particles ("collisions"). It is usually referred to as free-free emission. The inverse process is called collisional damping or free-free absorption. Since the energy of the emitted particle $E = \hbar\omega$ is not larger than the energy of the incoming particle $E_{\rm kin}$, the continuous bremsstrahlung spectrum is limited by

$$\omega \leq \omega_{\rm max} = \frac{E_{\rm kin}}{\hbar}. \tag{31}$$

The process may be treated classically if $\lambda_{\rm B} \ll r_0$, where $\lambda_{\rm B}$ is the de Broglie wavelength

$$\lambda_{\rm B} = \frac{\hbar}{m_{\rm e}|\mathbf{v}|} \tag{32}$$

and r_0 the distance of the closest approach. Since

$$r_0 \sim \Delta E \sim \frac{Ze^2}{E_{\rm kin}}, \tag{33}$$

one can write the condition for classical treatment as

$$v \ll \frac{2Ze^2}{\hbar}. \tag{34}$$

Thus, bremsstrahlung may be described classically for $\omega \ll \omega_{\rm max}$. In this case the radiation becomes of the dipole type.

One can in fact neglect radiation due to collisions between identical non-relativistic particles. Only quadrupole emission occurs in this case, being $(v/c)^2$

weaker than that of dipole emission. The dipole moment of a pair of identical particles equals

$$\mathbf{d} = Ze(\mathbf{r}_1 + \mathbf{r}_2), \tag{35}$$

where $\mathbf{r}_i$ are the radius vectors of the particles. If no external force is present, then

$$\ddot{\mathbf{R}} = 0 \tag{36}$$

with $\mathbf{R} = \mathbf{r}_1 + \mathbf{r}_2$ and thus

$$\ddot{\mathbf{d}} = 0. \tag{37}$$

Electron-electron encounters are extensively described in Dawson [32, Ch. IX] or Haug [47]. Furthermore, bremsstrahlung by heavy particles may as well be neglected due to the small accelerations.

An accelerated electron radiates at a rate

$$P = \frac{2}{3}\frac{e^2|\dot{\mathbf{v}}|^2}{c^3}, \tag{38}$$

which is the *Larmor formula* with

$$|\dot{\mathbf{v}}| = \frac{Ze^2}{m_\mathrm{e} r^2}, \tag{39}$$

where Z is the charge of the accelerating ion and r the distance between the ion and electron. Assuming uniform densities n_e and n_i and integrating Eq. (38) gives the total power radiated of all encounters

$$P_\mathrm{tot} = \frac{2Z^2e^6 n_\mathrm{i} n_\mathrm{e}}{3c^3 m_\mathrm{e}^2} \int_{r_0}^{\infty} \frac{4\pi}{r^2} dr = \frac{8\pi}{3}\frac{Z^2e^6 n_\mathrm{i} n_\mathrm{e}}{m_\mathrm{e}^2 c^3 r_0}. \tag{40}$$

The integral diverges for $r \to r_0$. Thus, at small distances, the classical treatment is no longer valid. Using λ_B as a quantum mechanical quantity gives

$$\frac{1}{k} = r_0 = \frac{\hbar}{p_\mathrm{e}} = \frac{\hbar}{m_\mathrm{e}}\sqrt{\frac{m_\mathrm{e}}{kT_\mathrm{e}}} \tag{41}$$

as an approximation. This leads to

$$P_\mathrm{tot} \cong \frac{16\pi^2 Z^2 e^6 n_\mathrm{i} n_\mathrm{e}}{3m_\mathrm{e} c^3 h}\sqrt{\frac{kT_\mathrm{e}}{m_\mathrm{e}}}. \tag{42}$$

For a quantum mechanical approach one obtains[3]

$$P_\mathrm{tot}^\mathrm{QM} = \sqrt{\frac{2\pi kT}{3m_\mathrm{e}}}\overline{g_\mathrm{ff}}\frac{32\pi^2 Z^2 e^6 n_\mathrm{i} n_\mathrm{e}}{3m_\mathrm{e} c^3 h}, \tag{43}$$

where $\overline{g_\mathrm{ff}}$ is the *Gaunt factor* of order 1.[4]

[3] See Dawson [32, Eq. (I.9)].

[4] In the Born approximation $\overline{g_\mathrm{ff}} = 1.103$.

The radiated energy of a single encounter is

$$U = \int_{-\infty}^{\infty} P(t)\, dt = 2 \int_{r_0}^{\infty} \frac{2Z^2e^6}{3m_e^2c^3r^4} \frac{dr}{\dot{r}}. \tag{44}$$

Omitting the calculation steps one obtains

$$U = \frac{2Z^2e^6}{3m_e^2c^3vb^3} \left[3\frac{b_0}{b} + \left(1 + 3\frac{b_0^2}{b^2}\right) \left\{ \frac{\pi}{2} + \arctan\left(\frac{b_0}{b}\right) \right\} \right], \tag{45}$$

where b is the impact parameter and

$$b_0 = \frac{Ze^2}{mv^2}. \tag{46}$$

For low frequencies one can use the *straight-line approximation* to compute U which follows from the fact that distant encounters ($b \gg b_0$) are more important than close encounters. Thus, the motion of the particle can, in zeroth order, be considered as constant rectilinear and the Coulomb force as a perturbing force. The unperturbed orbit is

$$\mathbf{r}^{(0)} = \mathbf{b} + \mathbf{v}t. \tag{47}$$

The perturbing force can be described by

$$\mathbf{F}^{(1)} = \frac{Ze^2r^{(0)}}{|r^{(0)}|}. \tag{48}$$

Since

$$\mathbf{F}^{(1)} = m_e\dot{\mathbf{v}}, \tag{49}$$

one obtains $P(t)$ which has to be integrated over dt and leads to

$$U = \frac{2e^2}{3c^3} \left(\frac{Ze^2}{m_e}\right)^2 \int_{-\infty}^{\infty} \frac{dt}{(b^2 + v^2t^2)^{3/2}} = \frac{\pi}{2} \left(\frac{2Z^2e^6}{3m_e^2c^3vb^3}\right). \tag{50}$$

A comparison with Eq. (45) for $b \gg b_0$

$$U = \frac{\pi}{2} \left(\frac{2Z^2e^6}{3m_e^2c^3vb^3}\right) \left(1 + \frac{8b_0}{\pi b} + \ldots\right) \tag{51}$$

shows that the straight-line approximation is useful for $b \gg (8/\pi)b_0$.

The frequency distribution for an isotropic plasma can be obtained from

$$U = \int_0^{\infty} U(\omega)\, d\omega, \tag{52}$$

where

$$U(\omega) = \frac{2}{3\pi} \frac{e^2n(\omega)}{c^3} |\dot{\mathbf{v}}(\omega)|^2. \tag{53}$$

The acceleration is given by

$$\begin{aligned}\dot{\mathbf{v}}(\omega) &= -\frac{Ze^2}{m_\mathrm{e}} \int\limits_{-\infty}^{\infty} \frac{\mathbf{b}+\mathbf{v}t}{(b^2+v^2t^2)^{3/2}}\, e^{i\omega t}\, d\omega \\ &= -\frac{2Ze^2\omega}{m_\mathrm{e}v^2}\left\{\frac{\mathbf{b}}{b}K_1^2\left(\frac{b\omega}{v}\right) - i\frac{\mathbf{v}}{v}K_0^2\left(\frac{b\omega}{v}\right)\right\},\end{aligned} \tag{54}$$

where K_ν is a MacDonald function with

$$K_\nu(xz) = \frac{\Gamma(\nu+\frac{1}{2})\,(2z)^\nu}{2x^\nu\Gamma(\frac{1}{2})} \int\limits_{-\infty}^{\infty} \frac{e^{\pm ixt}}{(t^2+z^2)^{\nu+1/2}}\, dt. \tag{55}$$

The MacDonald functions K_0 and K_1 may be approximated by [78]

$$K_0(x) \approx \ln\left(\frac{2}{x}\right) - 0.5772 + \ldots, \tag{56}$$

$$K_1(x) \approx \frac{1}{x} \tag{57}$$

for $x \ll 1$ and by

$$K_0(x) \approx K_1(x) \approx \sqrt{\frac{\pi}{2x}}\frac{1}{\mathrm{e}^x} \tag{58}$$

for $x \gg 1$. Thus, one obtains

$$U(\omega) = \frac{8}{3\pi}\frac{n(\omega)Z^2e^6\omega^2}{c^3m_\mathrm{e}^2v^4} \begin{cases} (v/b\omega)^2 & \text{for} \quad b\omega/v \ll 1, \\ \pi(v/b\omega)e^{-2b\omega/v} & \text{for} \quad b\omega/v \gg 1. \end{cases} \tag{59}$$

Finally, one may calculate the emissivity j_ν. For a medium with distribution function f, the emissivity j_ν is given by

$$j_\nu = \int P_\nu f(\mathbf{p},\mathbf{r},t)\, d^3p\, d\Omega. \tag{60}$$

This may be rewritten such as

$$j_\nu = N_+ \int \kappa_\nu v f(\mathbf{p})\, d^3p, \tag{61}$$

since

$$\kappa_\nu = 2\pi \int P_\nu b\, db, \tag{62}$$

where b is the impact parameter and κ_ν the effective spectral power. N_+ is the number of particles that the electrons interact with. Assuming an isotropic particle distribution $f(\mathbf{p})$, the emissivity is also isotropic

$$j_\nu = N_+ \int\limits_{p_\mathrm{min}}^{\infty} \kappa_\nu v f(p) p^2\, dp, \tag{63}$$

where $p_{\rm min} = \sqrt{2\hbar\omega m_{\rm e}}$ for a non-relativistic particle, since

$$E_{\rm kin} = \hbar\omega = \frac{p^2}{2m_{\rm e}}. \tag{64}$$

According to Zheleznyakov [118], in a non-relativistic plasma with temperature

$$T \ll \frac{\pi e^4 Z^2 m_{\rm e}}{2k\hbar^2} \tag{65}$$

the emissivity at frequencies

$$\omega \ll \frac{(8kT)^{3/2}}{\pi^{3/2}\sqrt{m_{\rm e}}e^2 Z} \tag{66}$$

may be calculated by

$$j_\nu \approx \frac{4}{3\pi}\sqrt{\frac{2}{\pi}}\frac{e^6 Z^2 N N_+}{\sqrt{kT}m_{\rm e}^{3/2}c^3}\ln\left[\frac{2(2kT)^{3/2}}{\delta^{5/2}e^2 Z\sqrt{m_{\rm e}}\omega}\right], \tag{67}$$

where $\delta = e^C$ with $C = 0.577$ the Euler constant. At frequencies

$$\frac{(8kT)^{3/2}}{\pi^{3/2}\sqrt{m_{\rm e}}e^2 Z} \ll \omega \ll \frac{4ckT}{\pi e^2 Z} \tag{68}$$

the emissivity is

$$j_\nu \approx \frac{4}{3}\sqrt{\frac{2}{3\pi}}\frac{e^6 Z^2 N N_+}{\sqrt{kT}m_{\rm e}^{3/2}c^3}. \tag{69}$$

At temperatures

$$T \gg \frac{\pi e^4 Z^2 m_{\rm e}}{2k\hbar} \tag{70}$$

one obtains

$$j_\nu \approx \frac{4}{3\pi}\sqrt{\frac{2}{\pi}}\frac{e^6 z^2 N N_+}{\sqrt{kT}m_{\rm e}^{3/2}c^3}\ln\left[\frac{4kT}{\delta\hbar\omega}\right]. \tag{71}$$

Note that Eqs. (67), (69) and (71) represent the total bremsstrahlung emission into two orthogonal polarizations

$$j_\nu = j_{\nu 1} + j_{\nu 2}. \tag{72}$$

Furthermore, Eqs. (67), (69) and (71) hold only in the Rayleigh-Jeans limit, i.e., $\hbar\omega \ll kT$. That gives

$$p_{\rm min} = m_{\rm e} v_{\rm min} \ll m_{\rm e} v_{\rm T}. \tag{73}$$

Thus, one can set $p_{\rm min} = 0$ in Eq. (63). For $\hbar\omega \simeq kT$, one needs to pay attention to an additional term $g(\omega, T)e^{-\hbar\omega/kT}$. The exponent arises from $p_{\rm min} \neq 0$ and the Gaunt factor $g(\omega, T)$ from the quantum effects for $p \sim p_{\rm min}$.

Finally, one may have a look at the bremsstrahlung emissivity expressed in quantum mechanical terms. For the Born approximation

$$v_{\mathrm{T}} \gg \frac{2Ze^2}{\hbar} \tag{74}$$

one obtains [118]

$$j_\nu = \frac{4}{3}\frac{e^6 Z^2 N N_+}{m_{\mathrm{e}}^2 c^3}\sqrt{\frac{m_{\mathrm{e}}}{2\pi kT}}g(\omega,T)e^{-\hbar\omega/kT}, \tag{75}$$

where

$$g(\omega,T) = \frac{\sqrt{3}}{\pi}K_0\left(\frac{\hbar\omega}{2kT}\right)e^{\hbar\omega/2kT}. \tag{76}$$

Using the approximation for the MacDonald function (56) for $\hbar\omega/2kT \ll 1$, this can be reduced to

$$g(\omega,T) \simeq \frac{\sqrt{3}}{\pi}e^{\hbar\omega/2kT}\ln\left(\frac{4kT}{\delta\hbar\omega}\right) \tag{77}$$

and Eq. (75) to Eq. (71). For $\hbar\omega/2kT \gg 1$ one obtains

$$g(\omega,T) \simeq \sqrt{\frac{3}{\pi}\frac{kT}{\hbar\omega}} \tag{78}$$

by using Eq. (58). The emissivity is thus

$$j_\nu \simeq \frac{4}{\sqrt{6}\pi}\frac{e^6 Z^2 N N_+}{m_{\mathrm{e}}^2 c^4}\sqrt{\frac{m_{\mathrm{e}}c^2}{\hbar\omega}}e^{-\hbar\omega/kT}. \tag{79}$$

2.3 Gyromagnetic emission

Gyromagnetic emission is caused by particles in spiraling motion in a magnetic field. Emission from non-relativistic particles is called *cyclotron* emission while emission from relativistic particles is called *synchrotron* emission. The transition between both definitions lies in the range of mildly relativistic velocities. In contrast to bremsstrahlung, gyromagnetic emission is anisotropic and in general elliptically polarized. Gyromagnetic emission by ions can usually be neglected because of the large ion masses.

Omitting most of the calculations that would exceed the bounds of space for this work, I only give the results for the emissivity and radiated power for cyclotron and synchrotron radiation. See Bekefi [8, Ch. 6], Boyd & Sanderson [19, Ch. 9.5], Rybicki & Lightman [93, Ch. 6] or Zheleznyakov [118, Ch. 5] for an extensive description of these phenomena.

The cyclotron radiation power for a electron moving in vacuum along a helical line can be obtained by [118]

$$P_\omega = \frac{e^2\omega_{\mathrm{B}}^2\beta_\perp^2}{2\pi c}(1+\cos^2\alpha)2^{-2s}s^6(s!)^{-2}(s\beta_\perp\sin\alpha)^{2s-2}, \tag{80}$$

where s describes the number of the harmonics, $\beta_\perp = v_\perp/c$, $\omega_\mathrm{B} = eB/m_\mathrm{e}c$ the cyclotron frequency and α the angle between the magnetic field and the wave vector. Eq. (80) implies that along the magnetic field ($\alpha = 0$) only cyclotron radiation at the fundamental ($s = 1$) is emitted. Furthermore, at angles $\alpha \neq 0$ elliptically polarized waves are emitted at all harmonics, whereas only linearly polarized waves are emitted by electrons with $\beta_\parallel = 0$ at $\alpha = \pi/2$.

Integrating Eq. (80) gives the total power of cyclotron radiation at the sth harmonic in vacuum

$$P = \frac{2e^2\omega_\mathrm{B}^2\beta_\perp^{2s}}{c}\frac{s^{2s+1}(s+1)}{(2s+1)!}. \tag{81}$$

Note that the value of P decreases with $\beta_\perp^{2s}$.

For a complete overview concerning the emissivities of the different emission modes of cyclotron radiation see Zheleznyakov [118, Ch. 5.2.3].

The study of the emission line can provide us with a wealth of information about the plasma. The electron pressure $p_\mathrm{e} = nkT$ can be calculated directly from the total energy under the line. Every line is broadened by several effects which provides further plasma quantities.

1. *Radiation broadening* results from the fact that a finite length wave train cannot have a pure frequency. This is due to the finite length of any real photon, since any atomic level in a line transition has a finite lifetime, except the ground state. The broadening arises from the interaction of the electromagnetic wave, i.e., the photon and an oscillating dipole, i.e., the absorbing atom. The process can therefore be described as a damped harmonic oscillator, thus by a Lorentz profile.

2. *Collisional broadening* arises from collisions of the electrons with ions and atoms with collision frequency ν. Thus, the spectral distribution becomes

$$P(\theta) = \frac{kT\omega^2\omega_\mathrm{p}^2}{4\pi^3c^3}(1+\cos^2\theta)\frac{\nu}{(\omega-\omega_\mathrm{B})^2+\nu^2}, \tag{82}$$

   where the last term is a Lorentzian profile. Hence, one can obtain ν from the shape of the line, i.e., the line width W, if collision broadening is dominant.

3. *(First order) Doppler broadening* is caused by the thermal motion of the electrons. This leads to a Gaussian shape of the line, i.e.,

$$P(\theta) \propto \exp\left[-\frac{mc^2}{2kT}\left(\frac{\omega-\omega_\mathrm{B}}{\omega_\mathrm{B}\cos\theta}\right)^2\right]. \tag{83}$$

   Hence, dominating Doppler broadening gives us the electron temperature. Combining Doppler and collisional broadening as the two most important mechanisms leads to a so-called *Voigt profile*:

$$P(\theta) \propto \exp^{-(\omega-\omega_\mathrm{B})^2} + (\omega-\omega_\mathrm{B})^{-2}. \tag{84}$$

As one can see from Eq. (84), the Doppler profile dominates the line centre and the Lorentz profile the line wings.

4. *Self-absorption of radiation*: In a tenuous plasma the radiation is described by Kirchhoff's law. As the optical depth τ increases due to increasing ω_p the line saturates, i.e., I_ω reaches the blackbody limit B_ω. A further increase of τ leads to a broadened line, because in a thermal plasma the intensity cannot exceed B_ω and thus the energy distributes itself over a wider frequency.

5. Further broadening processes are *relativistic change of mass* (or *second order Doppler broadening*), *plasma dispersion effects* and *rotational broadening*. See Bekefi [8] or Gray [42] for an overview.

If one leaves the non-relativistic case and approaches mildly relativistic velocities, the cyclotron emission spectrum changes radically: Higher harmonics of ω_B begin to contribute and for ultra-relativistic electrons most of the energy is emitted in higher harmonics. For 25 keV electrons, 50% of the energy is in higher harmonics, for 50 keV electrons it is 94%. Another characteristic is that the emission lines of the harmonics are no longer separated by $\Delta\omega \sim \omega_\mathrm{B}$, but by $\Delta\omega \sim \omega_\mathrm{B}\sqrt{1-\beta^2}$. The discrete spectrum for non-relativistic electrons becomes thus a more or less continuous spectrum for highly relativistic electrons.

The synchrotron spectrum for low frequencies

$$\omega \ll \omega_\mathrm{c} = \frac{3}{2}\omega_\mathrm{B}\left(\frac{E}{m_\mathrm{e}c^2}\right)^2 \tag{85}$$

with E the electron energy is given by [118]

$$P_\omega \approx \frac{\sqrt{3}}{2\pi}\frac{e^2\omega_\mathrm{B}}{c}2^{2/3}\Gamma(2/3)\left(\frac{\omega}{\omega_\mathrm{c}}\right)^{1/3}, \tag{86}$$

where Γ is the gamma function. The value of P_ω reaches the maximum value

$$P_\omega^\mathrm{max} \approx \frac{1.6}{2\pi}\frac{e^2\omega_\mathrm{B}}{c} \tag{87}$$

at

$$\omega_\mathrm{max} \approx 0.3\omega_\mathrm{c} \approx \frac{1}{2}\omega_\mathrm{B}\left(\frac{E}{m_\mathrm{e}c^2}\right)^2 \tag{88}$$

and decreases exponentially for $\omega \gg \omega_\mathrm{c}$:

$$P_\omega \approx \frac{\sqrt{3}}{2\pi}\frac{e^2\omega_\mathrm{B}}{c}\sqrt{\frac{\pi}{2}\frac{\omega}{\omega_\mathrm{c}}}e^{-\omega/\omega_\mathrm{c}}. \tag{89}$$

For a complete overview of the emissivities of the different emission modes for synchrotron radiation see Zheleznyakov [118, Ch. 5.2.4].

2.4 Čerenkov emission

In order to radiate in vacuum, a charged particle must move non-uniformly. However, a uniformly moving charge may also radiate in a medium under certain circumstances. This effect was discovered by Vavilov and Čerenkov and is unfairly named only *Čerenkov radiation.*

Consider a non-relativistic electron moving with velocity $\mathbf{v}$ in a medium with refraction index $n_j(\omega)$. If the electron emits a photon, the process can be described by the following conservation laws:

$$\frac{1}{2}m_e v^2 = \frac{1}{2}m_e v_1^2 + \hbar\omega, \tag{90}$$

$$m_e\mathbf{v} = m_e\mathbf{v}_1 + \hbar\mathbf{k}_j, \tag{91}$$

where $\hbar\omega$ and $\hbar\mathbf{k}_j$ are the photon energy and momentum, respectively. Substituting $\mathbf{v}_1 = \mathbf{v} + \Delta\mathbf{v}$ into Eqs. (90) and (91) one obtains

$$m_e\mathbf{v}\Delta\mathbf{v} + \frac{1}{2}m_e(\Delta\mathbf{v})^2 + \hbar\omega = 0, \tag{92}$$

$$m_e\Delta\mathbf{v} + \hbar\mathbf{k}_j = 0. \tag{93}$$

Let us assume $|\Delta\mathbf{v}| \ll |\mathbf{v}|$, i.e., the velocity change due to the emission of the photon is small. Thus, we can neglect the second term in Eq. (92). By eliminating $\Delta\mathbf{v}$ from Eqs. (92) and (93) we finally obtain a condition for the Vavilov-Čerenkov effect:

$$\omega = \mathbf{k}\mathbf{v}. \tag{94}$$

By introducing $k_j = n_j\omega/c$, $v = \beta c$ and the angle θ between $\mathbf{k}$ and $\mathbf{v}$ one can rewrite condition (94) as

$$\beta n_j \cos\theta = 1. \tag{95}$$

Furthermore, we can transform this into

$$v_{\mathrm{ph}} = v\cos\theta \tag{96}$$

by using $v_{\mathrm{ph}} = c/n_j$. At fixed v and v_{ph} the conditions (94), (95) and (96) define the "Čerenkov cone". Within this cone radiation is due to Čerenkov emission. Since $v < c$ and $\cos\theta \leq 1$, Čerenkov radiation can be generated only for $v_{\mathrm{ph}} < c$.

Omitting the calculation steps, the spectral power of Čerenkov radiation can be calculated by [118]

$$P_\omega = \frac{e^2\omega}{v\epsilon(\omega)}, \tag{97}$$

where $\epsilon(\omega)$ is the dielectric permeability of the isotropic plasma. The Čerenkov emissivity by electrons in a equilibrium plasma can be obtained from [118]

$$j_\omega = \frac{e^2\omega N}{(2\pi)^{3/2}v_{\mathrm{T}}\epsilon(\omega)}\exp\left[-\frac{m_e v_{\mathrm{ph}}^2}{2kT}\right]. \tag{98}$$

Note that the equation above is only valid in a non-absorbing medium and if Landau damping is weak.

3 Review of solar radio bursts

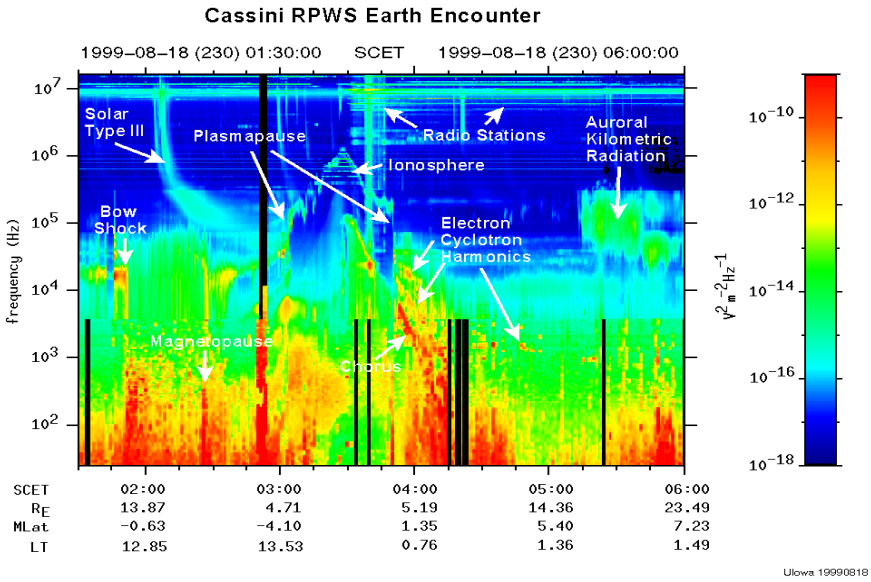

Figure 1: Overview of natural and artifical radio emissions observed by the Cassini spacecraft during an Earth flyby. August 18, 1999. Taken from http://www-pw.physics.uiowa.edu/~wsk/cas/Cassini-Earth.gif.

Figure 1 shows a dynamic spectrum obtained by the Cassini spacecraft during an Earth flyby. It gives an overview of the frame in which solar radio bursts fit in. As one may see, besides solar radio bursts there exist many different radio emissions, both artificial and natural. The natural radio sources in the solar system are of course Earth, Jupiter and the strongest radiator, the Sun. One may divide the solar radiation into a disturbed and quite part (thermal bremsstrahlung), characterized by the 11-year-activity cycle. Solar radio bursts are part of the radio emission of the disturbed Sun.

In this Chapter, I summarize the most important characteristics of solar radio bursts of type I to V, type U(N) and spike bursts as well as radio bursts originating from Jupiter. In Chapter 4 type II and III bursts are represented as a detailed example.

There exists a host of literature dealing with solar radio bursts. For a general overview see Krüger [68], McLean & Labrum [77] or Zheleznyakov [116]. The theoretical background is presented by Bekefi [8], Benz [10], Kaplan & Tsytovich [58], Melrose [78, 80], Rybicki & Lightman [93] or Zheleznyakov [118], for example.

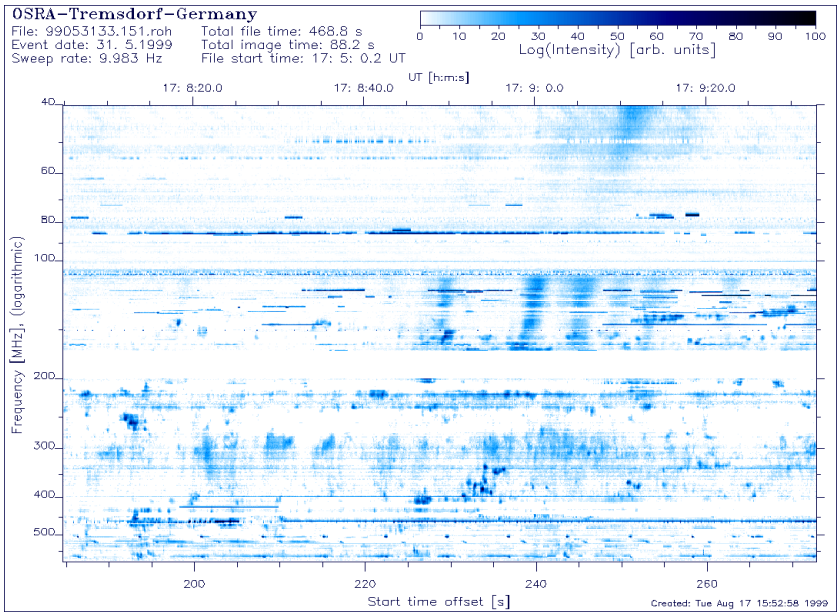

Figure 2: Solar radio noise storm. OSRA (Solar Radio Observatory Potsdam-Tremsdorf, Germany. OSRA consists of 4 sweep spectrographs with 10 sweeps per second in the frequency ranges 40-90 MHz, 100-170 MHz, 200-400 MHz and 400-800 MHz). May 31, 1999. Taken from http://www.aip.de/groups/osra/gallery/99053133_sp4.gif.

3.1 Type I bursts

Type I emissions, mainly occurring in storms, consist of a continuous part and short duration, narrowband bursts, i.e., $\Delta f/f \leq 1$, occurring either together or separately. They are highly polarized ($\sim 100\%$) in the O-mode and appear to be at the fundamental of the local plasma frequency. Melrose [79] suggested a model with fundamental emission and negligible second harmonic. See also Benz & Wentzel [69, pg. 251-254] for a summary of their theory. The main problem with confirming such theories is the missing identification of any exciting agent. Elgarøy [40] summarized existing attempts at explaining solar noise storms.

3.2 Type II bursts

Coronal shock waves can be caused by solar flares and/or coronal mass ejections (CME) [3]; see Schwenn & Marsch [95] for a summary. The exact relation between CMEs, flares and type II bursts is still a matter of debate, since the subject seems to be quite involved [60]. The shock waves excite in their turn type II bursts, see Figure 3.

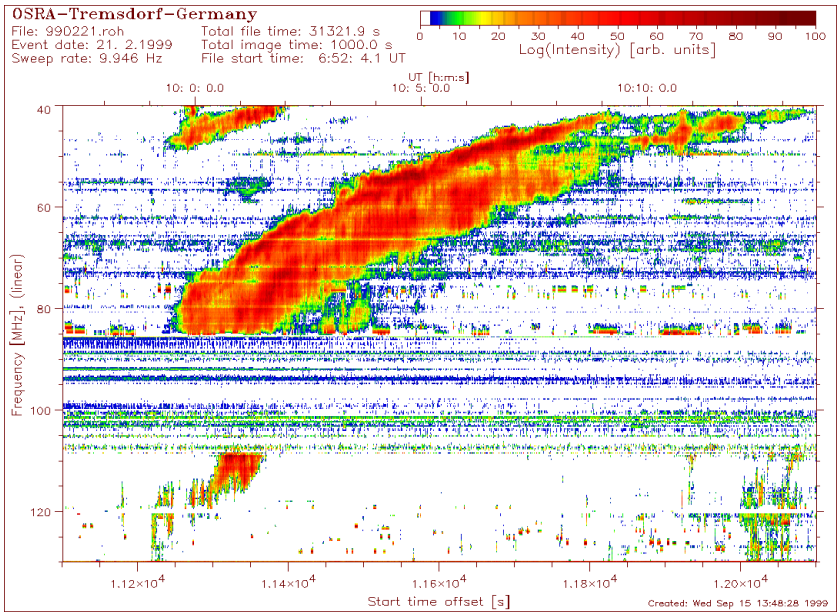

Figure 3: Type II burst with fundamental-harmonic structure and band-splitting. OSRA. February 21, 1999. Taken from http://www.aip.de/groups/osra/gallery/990221_4.gif.

The mechanism of generation of type II bursts is still a matter of ongoing research. The problem is to determine which coronal shock waves are associated with these bursts. The relation between type II bursts and Moreton waves is well accepted [83]. They represent shock waves in the chromosphere ($T \sim 10^4$ K) and have a mean speed of about $\bar{v} \sim 650$ km/s. Newer results also suggest an association with coronal transient waves [73] ($T \sim 10^6$ K, $\bar{v} \sim 250$ km/s). They were named EIT-waves, see Figure 4, due to the observations by the SOHO-EIT instrument. About 90% of all type II bursts are associated with EIT waves [62]. Unfortunately, the observation material is not sufficient for judging if EIT waves may be considered as the coronal counterpart of the chromospherical Moreton waves.

Another critical point is the relation between flares and CMEs [67]. Although it is well-accepted that *interplanetary* shocks are driven by CMEs [25], it becomes more and more likely that *coronal* shocks are mostly driven by flares [63, 105]. Thus, the essential question is to determine the region where the emission arises and the association with the flare active region.

There have been only a few in-situ measurements, since CMEs seldom reach Earth's orbit. Most CMEs fade away before they reach Earth's orbit. While for $f \sim 400$ MHz the radiation originates from the solar corona, for $f \sim 20$ kHz the radiation is located at 1 AU, i.e., Earth's orbit.

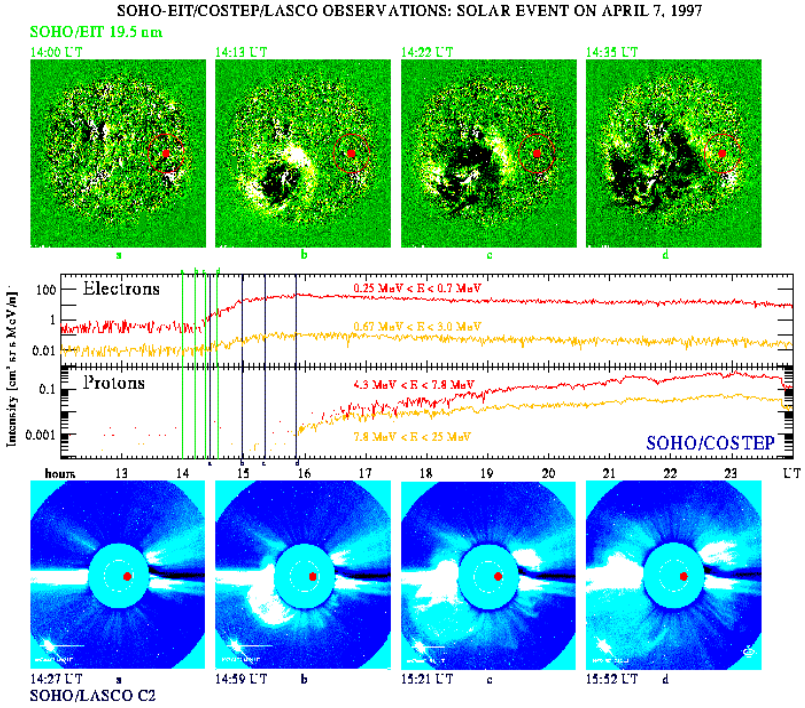

Figure 4: Coronal shock wave event. SOHO. April 7, 1997. Taken from http://sohowww.nascom.nasa.gov/gallery/COSTEP/cos005.gif.

The bursts occur as emission stripes in dynamic radio spectra and have narrow bandwidths, i.e., $\Delta f/f \leq 1$. They drift slowly from high to low frequencies, i.e., $D_\mathrm{f} \sim -0.1\,\mathrm{MHz\,s^{-1}}$. The drifting rate can be calculated by

$$D_\mathrm{f} = \frac{f}{2}\frac{1}{N}\frac{dN}{dr}V_\mathrm{r}, \tag{99}$$

where N is the particle density and V_r the radial source velocity.

The main component is also called "backbone" and is weakly circularly polarized ($\sim 5\%$) in the O-mode. Higher time and frequency resolution provides some fine structures, for example the so-called "herringbones" which are rapidly drifting, broadband emission stripes shooting out of the "backbone" at higher and lower frequencies. About 20% of type II bursts show "herringbone" fine structure. These emissions represent the signature of type III bursts which can be considered as electrons that are accelerated by the shock wave. They are slightly higher polarized than the "backbone" and show also a fundamental-harmonic fine structure. Further fine structures are band-splitting, see Figure 3,

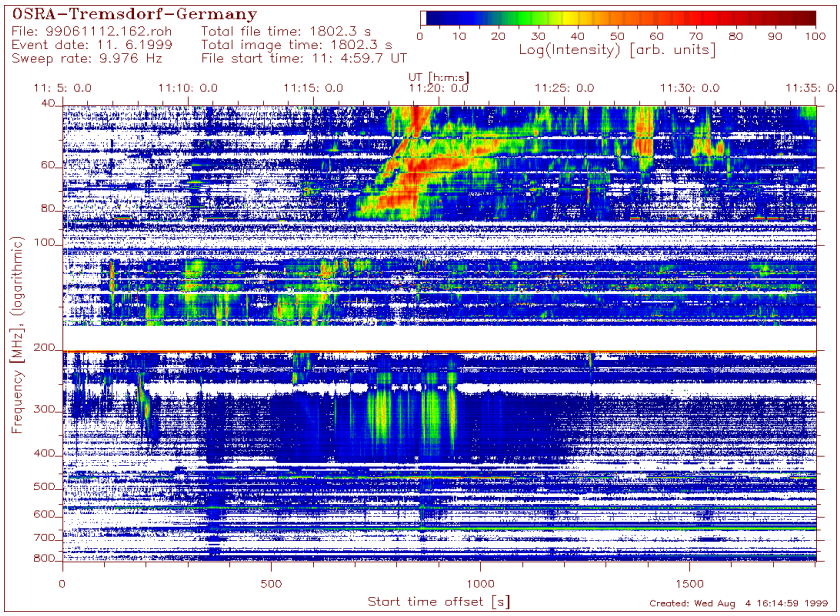

Figure 5: Type II burst with typical precursor pattern. OSRA. June 11, 1999. Taken from http://www.aip.de/groups/osra/gallery/99061112.gif.

and multiple-lane structure.[5]

Some of the observed type II bursts show three fundamental bands at a frequency ratio of about 3:2:1, see Figure 3. The emission, described in Chapter 4.2, and acceleration processes, described in Chapter 4.1, are still subject to research. General consideration favours that type II bursts are generated by shock drift acceleration [54]. This is only valid for quasi-perpendicular shocks. Mann et al. [72] suggested a model for quasi-parallel shocks which also gives an explanation for the location of the radio emission. High and low frequency wave components are needed for the fundamental type II emission. Both components appear commonly only in the vicinity of the transition region of the shock. Thus, one concludes that this is the locus of generation of these bursts and that the instantaneous bandwidth represents the density jump across the shock wave. The density jump can be calculated by the Rankine-Hugoniot relations [89].

The emission at the fundamental is assumed to be caused by the interaction of Langmuir waves L with ion sound waves S which leads to a transverse electromagnetic wave T ($L + S \rightarrow T$). The Langmuir waves in their turn are assumed to arise from excitation by the shock wave. Since $\omega_S \ll \omega_L$, one obtains $\omega_T \simeq \omega_L$. The emission at the second harmonic arises from the interaction of two Langmuir waves ($L_1 + L_2 \rightarrow T_{2L}$). The emission process for the third

[5] See Holman & Pesses [54] for different fine structure configurations.

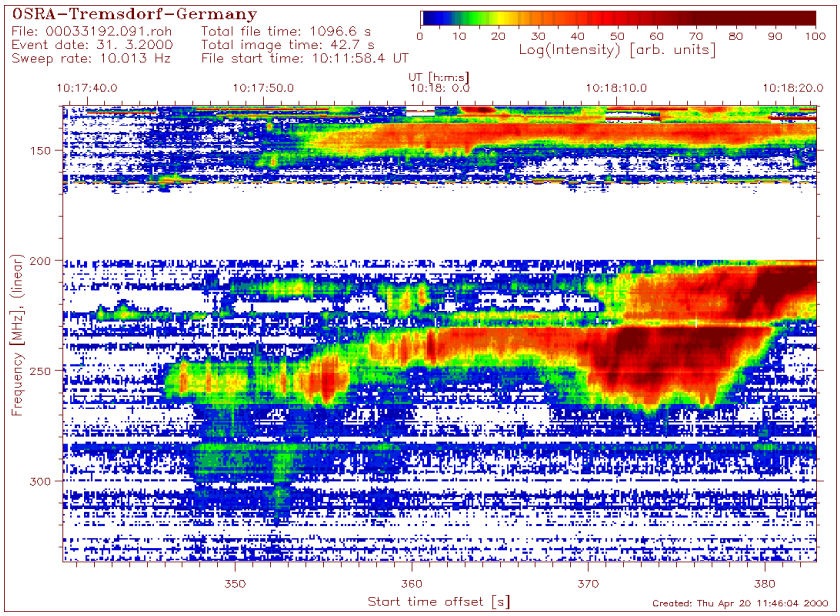

Figure 6: Arc pattern. OSRA. March 31, 2000. Taken from http://www.aip.de/groups/osra/gal_2000/00033192_b.gif.

harmonic is quite controversial [120]. See Chapter 4.2 for a deeper treatment.

Newer research [61] locates the type II source above active regions. These results were obtained by using X-ray observations made with the *Yohkoh* satellite. Furthermore, flare-related phenomena preceding type II emissions were observed: The type II precursor and the arc pattern. This has provided new knowledge concerning electron injection and emission processes.

The precursor appears as a group of fast drift bursts. They occur in coronal loops from the impulsive flare phase to the onset of the type II burst and their spectral location could be found near the backward extrapolated type II lanes. The fact that these bursts are found between the site of the Hα emission and the type II burst onset implies the idea that the precursor is a result of the disturbance which later becomes the exciter of the type II emission. However, one cannot determine if the electron beams, which are assumed to give rise to the precursor, are accelerated by the disturbance or if the disturbance suppresses a part of the spectrum. Figure 5 shows a type II burst starting at 11:14 UT at $f \sim 200\,\mathrm{MHz}$ and typical precursor pattern at 11:08 UT – 11:12 UT around $f \sim 150\,\mathrm{MHz}$.

The arc pattern consists of short-duration series of narrow-band bursts occurring immediately before the type II onset and ending between the split bands of the type II burst. Due to the inverted U-shaped envelope it was named *arc*, see Figure 6. It shows fundamental-harmonic fine structure, but no band split-

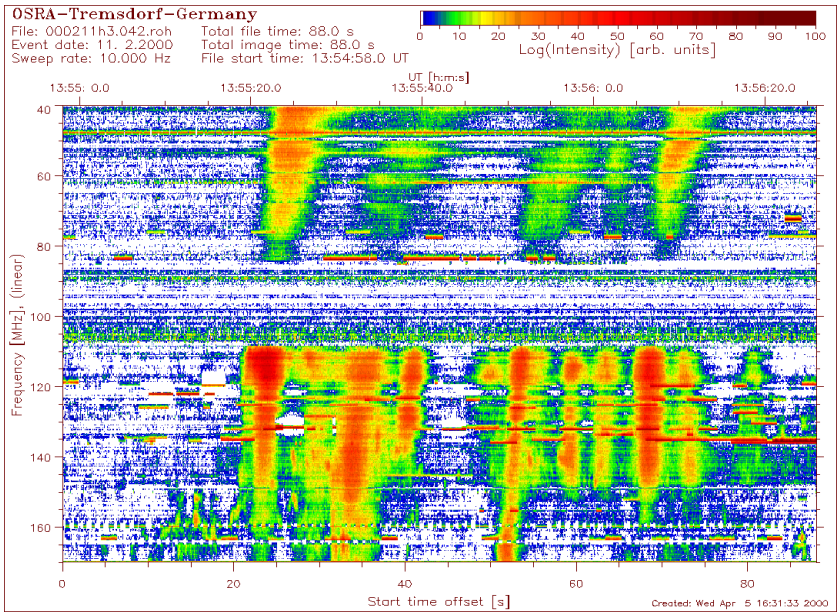

Figure 7: Group of type III bursts. OSRA. February 11, 2000. Taken from http://www.aip.de/groups/osra/gal_2000/000211h3.gif.

ting. X-ray observations revealed that the source is located above the coronal loops creating the precursor and near the locus of type II emission. Due to the shape and no band splitting one may assume that the emission process for the arc is quite different than for the type II emission. Furthermore, the arc source is located close to, but different from, the type II source which implies that the arc might be due to a change of propagation conditions from closed to open field lines. Observations of type III bursts associated with arc structures underline this idea. See Klassen et al. [61] for an extensive description of the precursor and arc phenomena.

Type II bursts were first observed at fixed frequencies simultaneously by Payne-Scott, Yabsley & Bolton in 1947 [87]. Later, dynamic spectra of type II bursts were obtained by Wild and others in the 1950s.

3.3 Type III bursts

These emissions, see Figure 7, can be considered as the signature of electron beam-driven radio bursts associated with flares, although not every flare is accompanied by a type III burst. This reflects the following steps of the flare phenomena:

1. the energy release mechanism

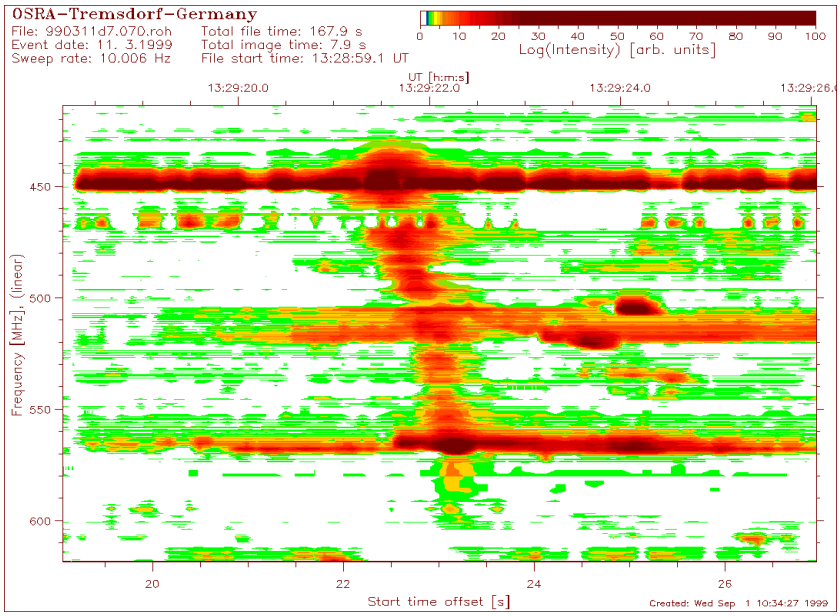

Figure 8: Reverse slope (RS) burst. OSRA. March 11, 1999. Taken from http://www.aip.de/groups/osra/gallery/990311d7.gif.

2. the acceleration process of the non-thermal particles

3. their propagation along open or closed field lines

4. the generation of the observed emission

As mentioned above, the main feature of type III events is the high drift rate $(df/dt) \sim 100$ MHz s^{-1} and their broad bandwidth. They occur over a frequency range of 8 GHz $\geq f \geq$ 10 kHz with corresponding speed of the exciting electrons of $0.2c \leq v \leq 0.6c$ given in most published papers, while Dulk et al. [37] mentioned a considerably lower value of $0.07c \leq v \leq 0.25c$. The bursts occur in groups of 10 or more (up to 100) during the impulsive phase of a flare and are common whenever an active region is present on the Sun.

The associated electrons ($\sim 10^{33}$/beam) propagate along open field lines. Travelling outward, they result in "normal" type III bursts, see Figure 7. Downward propagating electrons lead to a so-called *reverse slope burst* (RS burst), see Figure 8. Furthermore, two electron beams travelling down- and upward, respectively, have been observed. They are so-called "bidirectional type III bursts" [92]. These "oppositely drifting pairs" provide a unique possibility to determine to plasma density in the acceleration source. This can be achieved by measuring the location of the separatrix. Aschwanden et al. [6] stated that the production of bidirectional beams is quite common. However, it is well-known

that upward propagating beams are more likely detected than downward propagating ones. This might be due to enhanced free-free absorption at higher decimetric frequencies or the finite distance necessary for the beam evolution, among other things. Benz et al. [11] observed type III bursts in the low corona up to $f \sim 8.4$ GHz.

As mentioned above, type III bursts are associated with flares. Extensive studies by Aschwanden et al. [5] showed a high correlation between clustering of type III bursts and hard X-ray (HXR) pre-burst structures, so-called "elementary flare bursts" [33]. Aschwanden also gives an overview of different timescales during particle acceleration:

1. total flare duration (enhanced HXR emission): ≈ 10 min
2. impulsive phases (occurrence of rapid HXR fluctuations and clustering of type III bursts): ≈ 1 min
3. modulation of acceleration efficiency (HXR "elementary bursts"): ≈ 5 s
4. period of single bursts (timescale on which an Alfvénic disturbance traverses the source): ≈ 1 s

These timescales were also reviewed by Sturrock et al. [99].

At metre and decametre wavelengths, type III bursts show a significant harmonic structure, while this is very rare at decimetre and kilometre wavelengths, see Figure 7. Type III are moderately circularly polarized at the fundamental ($\sim 50\%$), emitting in the O-mode. The harmonics are less polarized than the fundamental, but in the same sense [14].

The interpretation of type III bursts proceeded quite slowly, as characterized by the so-called "Sturrock's dilemma" [98]. Sturrock showed that, using standard parameters, the distance at which the injecting electron beam loses all its energy to waves was much shorter than observed. Several attempts were made to resolve this dilemma but none of these delivered a complete solution to the problem. The "standard model" states that the electron beam suffers only Coulomb and weak wave losses, i.e., it can travel large distances almost undisturbed. This problem was recently solved by Thejappa et al. [101] by using measurements made by ULYSSES. The question still remains how the particles are injected from the flare release volume and how the inhomogeneous magnetic field influences the observed emission.

In 1995 Vlahos and Raoult [104] suggested a new model containing several beams injected in different fibres of the magnetic field. Their simulations led to results well-related to observations. The number of injected beams may be related to the well-known division of type III bursts in "isolated", "groups" and "groups with continuum". This model was improved by Isliker et al. [55].

Fast drifting type III bursts, called type IIId, present a special subclass and form maybe a solar burst class on their own. Type IIId bursts drift faster than "normal" type III bursts, occur sometimes before a "normal" type III burst and arise from the relativistic head of a electron beam [88].

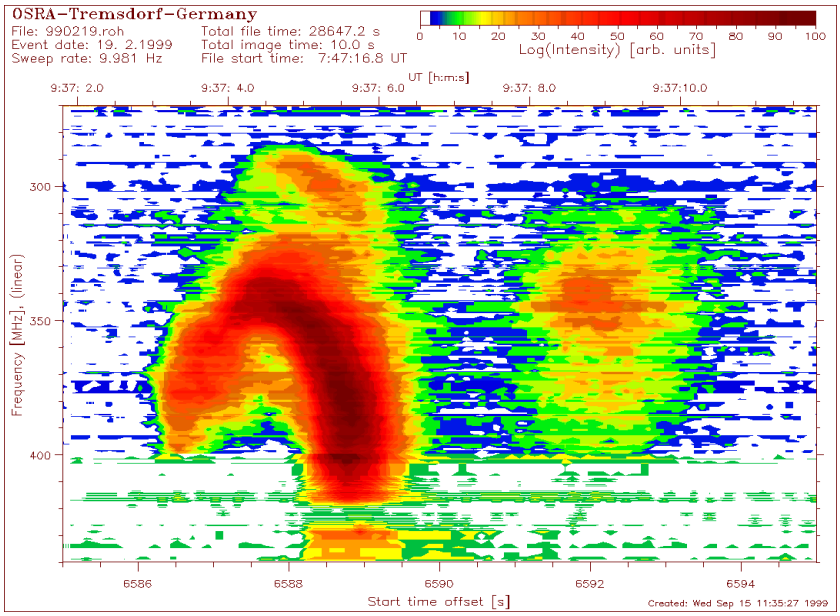

Figure 9: U(N) burst. OSRA. February 19, 1999. Taken from http://www.aip.de/groups/osra/gallery/990219.gif.

Another subclass are type IIIb bursts: Chains of split-pair and narrow-band bursts (so-called stria-bursts) that appear on high-resolution and high-sensitivity spectra. Type IIIb bursts are supposed to be precursors to "normal" type III bursts [34] and are very short bursts (< 1 s) with a narrow bandwidth of about 15 to 100 kHz. They are nearly as common as type III bursts and highly circularly polarized ($\sim 100\%$).

Type III bursts were classified by Wild [112]. He also suggested that these emissions are due to streaming electrons – a suggestion which is still valid today.

3.4 U(N) type bursts

The so-called U(N) emissions, Figure 9, are also due to suprathermal electrons, just as type III bursts. In contrast to type III bursts, these electrons are travelling along *closed* magnetic field lines [59]. The dynamic spectrum of such a burst looks like an inverted letter *U* and thus this component has been given the name of an *U burst* after its discovery by Maxwell and Swarup in 1958 [20].

The frequency drift inversion of U bursts can be explained by the fact that the causing electrons first rise into the upper layers of the corona and then move down again. Observations reveal a strong relation to flares (more than 80% of U bursts are accompanied by flares). Another interesting feature is that the

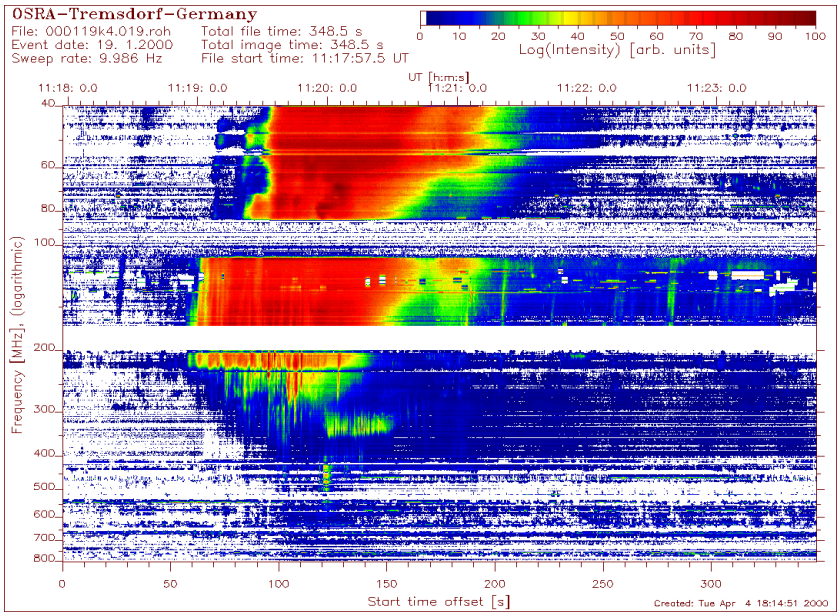

Figure 10: Type IV burst. OSRA. January 19, 2000. Taken from http://www.aip.de/groups/osra/gal_2000/000119k4.gif.

"turn" frequency (which is related to the maximum altitude) is connected to the maximum drift rate $|df/dt|_{\max}$. This represents on the other side the radial velocity of the agent. Observations made by Dumas et al. [39] in 1982 revealed a third ascending branch following a U type burst. So this event was named *N* type burst and it is believed to represent radio emission of electrons trapped and mirrored in solar magnetic loops.

Hillaris, Alissandrakis and Vlahos [52] suggested a model for N type bursts in 1988. They showed that under coronal conditions one can treat a thermal cloud injected at one end of a large loop (with a length of the order 2×10^5 km) by using the free streaming drift approximation. Much research has to be performed in that area.

Karlický et al. [59] studied the trajectories of superthermal electrons in coronal loops by using a 1-D test particle model. They found that U(N) bursts can arise not only from mirroring in a convergent magnetic field, but also by scattering of the electrons by an enhanced whistler turbulence in a loop leg. The model was successfully proved on an observed U(N) burst (February 23, 1993).

U bursts have a lower occurrence rate than type III bursts. Especially in the solar wind, U bursts are very rare. Note that a U burst disappearing before or at the turning point is often named *J* burst.

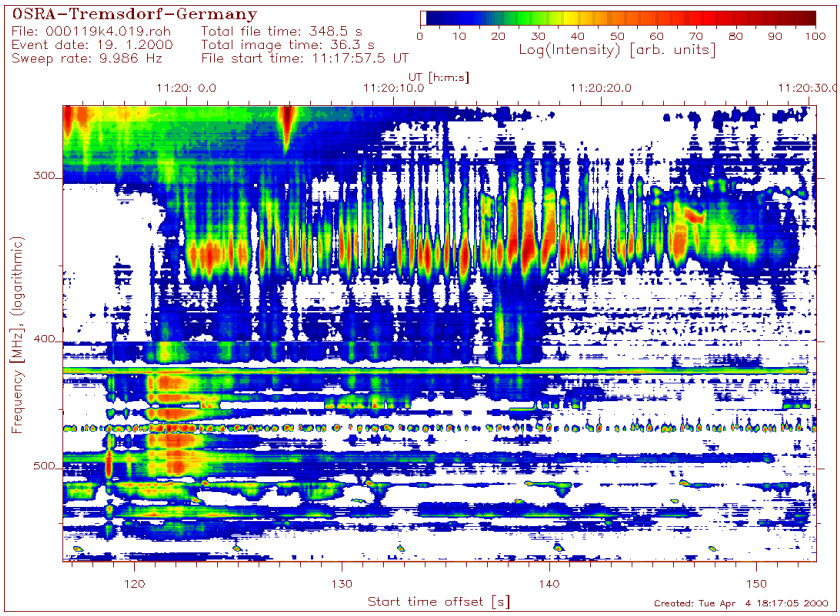

Figure 11: Type IV burst with pulsation fine structure. OSRA. January 19, 2000. Taken from http://www.aip.de/groups/osra/gal_2000/000119k4_1.gif.

3.5 Type IV bursts

Type IV bursts, Figure 10, are complex broadband bursts which are strongly polarized. In the classical picture, electrons are accelerated in the current sheet and then trapped in large magnetic arches. Known features of these events are pulsations with a sharp cut-off, Figure 11, and the so-called "zebra patterns", Figure 12, which represent fibres oscillating in frequency and can be observed in highly resolved dynamic spectra [15]. Furthermore, so-called intermediate drift (IMD) fine structures were observed, see Benz & Mann [12] for a review on the various theories on IMD.

On 17 February 1992, new fine structures in the "zebra" pattern were discovered [30]: A rapid frequency shift of the whole "zebra pattern" by an amount comparable to the stripe separation. Furthermore, a sub-splitting of a stripe into two stripes was observed. Interpretation has still to be made, but the most common idea is that these fine structures are caused by particle injection into a magnetic trap. Zebra patterns are quite complex structures and hence, numerous theories have been suggested, see Chernov et al. [30] for an overview. The main idea behind these models is electrostatic emission at twice the plasma resonance:

$$\omega_{\mathrm{uh}} = \sqrt{\omega_{\mathrm{p}}^2 + \omega_{\mathrm{B}}^2} = 2\omega_{\mathrm{B}}, \tag{100}$$

with ω_{uh} the upper hybrid frequency, ω_{p} the plasma frequency, ω_{B} the cy-

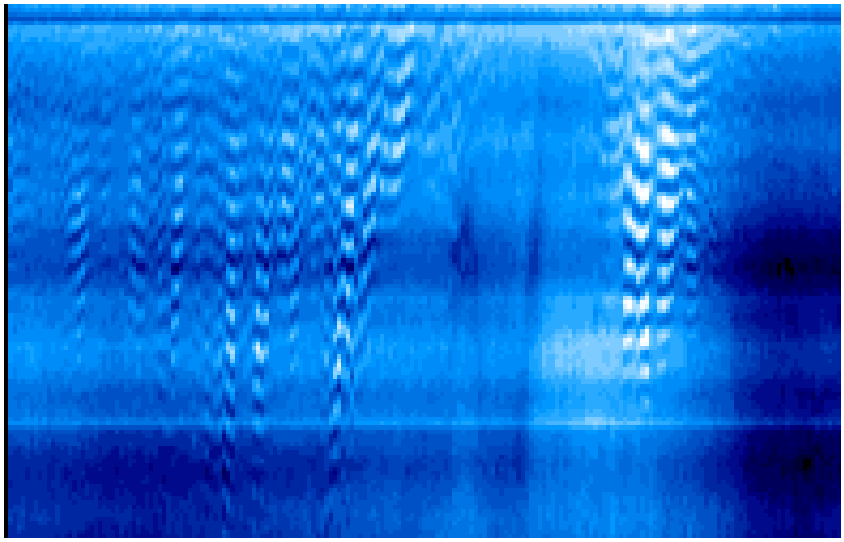

Figure 12: Zebra fine structure in a type IV burst (f vs. t). OSRA. 260 Mhz $< f <$ 360 Mhz. August 17, 1998. 07:06:21 - 07:07:07 UT. Taken from http://www.aip.de/groups/osra/gif_input/980817-0706s.gif.

clotron frequency and s an integer harmonic number. Furthermore, a long-lasting "evolving emission line" (EEL) was discovered. It appeared as a narrow band emission ($\Delta f \sim 10$ MHz) oscillating sinusoidally in frequency. The EEL is possibly due to coherent emission, since incoherent emission would generate much broader spectra. The particular emission process is not understood yet.

Chernov et al. [30] compared two theories with the new observations: The $L + W \rightarrow T$ model by Chernov [29] and the *Winglee & Dulk* model [113]. The first model uses Langmuir wave – whistler coupling at normal and anomalous Doppler resonances. It can explain all fine structures and leads to an expected magnetic field of 11×10^{-4} T in the source. The latter model is characterized by electron-cyclotron maser emission of upper-hybrid waves at double plasma resonance. This model can most possibly explain the EEL originating in the dense current sheet.

3.6 Type V bursts

Type V bursts appear as diffusive broadband quasi-continuous emission after some type III bursts. They were classified by Wild et al. [20, pg. 176] due to their wide spectra, their long duration (a few minutes) and their association with type III bursts. Type V bursts were reviewed by Suzuki & Dulk [77, Ch. 12.10]. Unlikely type III bursts, that are associated with the impulsive phase of HXR bursts ($E \leq 100$ keV), type V bursts are correlated with the gradual decay phase ($E \sim 30$ keV) [90]. Due to the broadband nature, no convincing fundamental-

harmonic fine structure has been found, although evidences were presented that both components are occasionally observable. Type V emissions are circularly polarized ($\leq 10\%$). Most surprisingly, the polarization of type V bursts preceded by a type III bursts shows an opposite sense than the type III polarization [38]. A change from O-mode in the type III burst to X-mode in the type V burst is favoured. This requires however an evolution of the angular distribution of Langmuir waves from angles of $\leq 20°$ to $\leq 60°$ from the magnetic field.

Raoult et al. [90] presented a model that claims that type III and V bursts are generated in the same coronal structures. The injected distribution of electrons consists of a spiky, energetic and a slowly evolving, less energetic part, representing type III and V emission, respectively. The two populations are coupled and reinforce each other. Thus, this could be the reason for the fact that type III and V bursts are mostly observed together. It is supposed that type V emission arises from electrons in high coronal loops adjacent to the open field lines traversed by the type III electrons.

3.7 Spike bursts

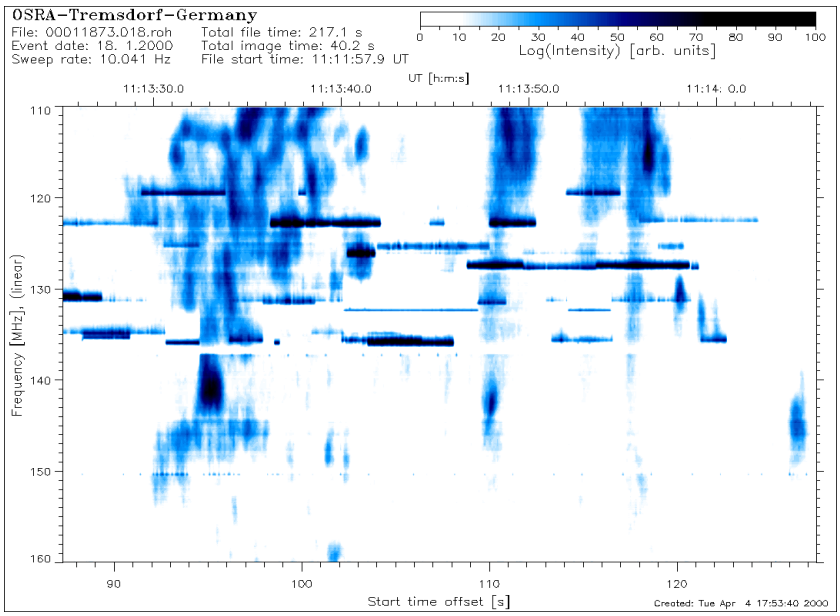

Figure 13: Spike bursts. OSRA. January 18, 2000. Taken from http://www.aip.de/groups/osra/gal_2000/00011873_1.gif.

Narrowband spike bursts, Figure 13, with a duration of a few tens of microseconds are another type of radio emission of the disturbed Sun correlated with HXR. They occur in groups with up to 10^4 bursts under a time period of

1 minute and show fine structure in frequency and fundamental-harmonic bands up to the sixth harmonic [43].

Metric spikes show a high correlation with metric type III bursts, they occur near the start of these type III bursts. It is not known if decimetric or microwave spikes are of the same physical manner. Metric spikes are always higher polarized than the type III emissions, sometimes showing opposite sign. A possible explanation of the strong association might be that the electron beam excites the type III bursts and earlier the spike emissions at higher frequencies. However, it might also be possible that these spikes are produced by wave turbulence within the acceleration region.

Decimetric millisecond spikes show the fastest fluctuations (< 200 ms) and the narrowest bandwidth ($\Delta f/f \approx 0.01 - 0.05$) of any radio bursts. From their bandwidth one may derive the extremely non-thermal brightness temperature ($T_{\mathrm{B}} = 10^{15}$ K) and the size of the sources (< 200 km) [9]. These bursts were found to be highly circularly polarized (up to 100%), emitting in the X-mode [44] and exhibiting fundamental-harmonic fine structure. Newer results show that in fact any polarization degree may occur with similar probability and that the polarization varies from the centre to the limb, i.e., the polarization degree tends to zero toward the limb [44]. Decimetric spikes may be classified according to their type III or IV association, respectively.

The emission may be due to two mechanisms: Synchrotron radiation or plasma emission associated with MHD and hydrodynamic shocks. Up to now, sufficient observational material to distinguish between these two mechanisms is not available [60].

3.8 Jovian radio emission

The low-frequency Jovian radio emission was discovered by Burke & Franklin in 1955 [21]. The radio spectrum of Jupiter spans the frequency range from 10 kHz to 3 GHz and is dominated by strong non-thermal radiation generated by the planet's inner magnetosphere and probably upper ionosphere.

Frequencies above 100 MHz are dominated by a continuous component generated by synchrotron radiation arising from trapped electrons between 1.3 and 3 $\mathrm{R_J}$. This component is characterized by a broad spectral peak at decimetric wavelengths (DIM), longitudinal asymmetries due to asymmetries in Jupiter's magnetic field and slow intensity variations.

The decametre wavelength (DAM) component between a few tenths of MHz and 39.5 MHz is Jupiter's strongest radio source. It exhibits a rich fine structure in frequency and time and is strongly dependent on the longitude of the observer. The DAM component is supposed to be generated near the electron cyclotron frequency, but neither location of the emission nor emission processes are determined.

At frequencies below 1 MHz, two components with spectral peaks at kilometric wavelengths (KOM) are significant. The bKOM component is bursty and broadbanded showing a strong association with the planetary rotation. The nKOM component is narrow banded and relatively weak with a peak near

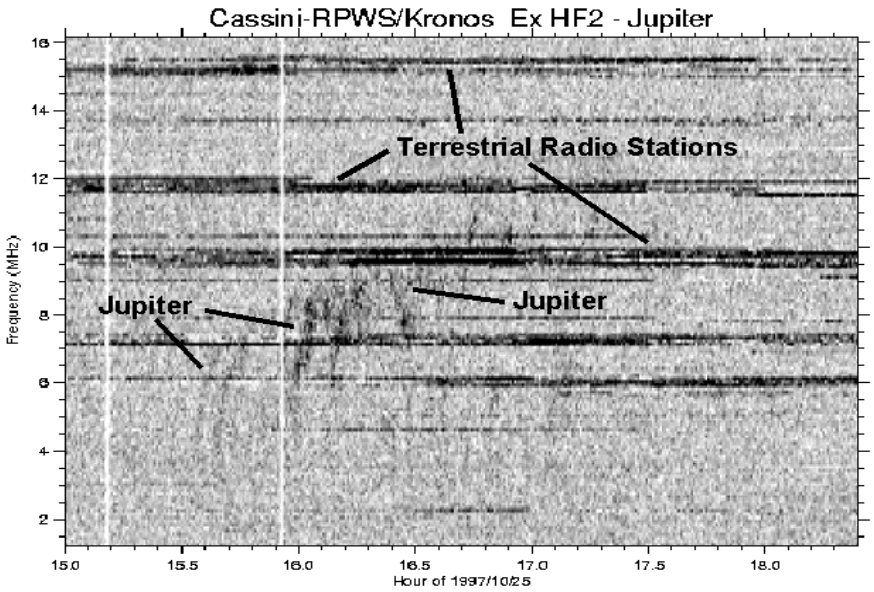

Figure 14: Jovian radio bursts observed by the Cassini spacecraft. October 25, 1997. Taken from http://www-pw.physics.uiowa.edu/~wsk/cas/kronos.gif.

100 kHz. It is supposed to arise from the outer part of the Io plasma torus (8 to 10 R_J) and is generated near the electron plasma frequency.

For a complete overview of Jovian radio emission I refer to Dessler [35].

3.9 The importance of low frequency radio astronomy from space for the research on solar bursts

The ionosphere of the Earth prevents ground measurements below a few MHz and has a certain influence (described by its extinction coefficient) on the observations through the measurement window. Thus, an observation station above the ionosphere could provide measurement possibilities undisturbed by the ionosphere and below a few MHz. In particular, type III bursts are observed below this limit. Furthermore, a higher spatial resolution provided by a radio interferometer, as ALFA [107, 110], could produce new insights into the relation of "backbone" and "herringbone" emissions or other fine structures such as band splitting. Polarigrammes, particularly with the novel polarimetry technique developed by Carozzi et al. [27] at IRFU, could be helpful to distinguish the different emission modes.

4 Solar type II/III bursts as a detailed example

Here I give an overview of acceleration mechanisms and emission processes responsible for the fundamental and harmonic emission in solar type II and type III bursts. Furthermore, collisionless shocks are described.

4.1 Acceleration mechanisms

The acceleration of the particles play an important role for the radiation in solar radio bursts. Here I present a short outline of different acceleration mechanisms such as shock drift acceleration, SLAMS, stochastic and shock drift acceleration.

4.1.1 Shock drift acceleration

All models for solar type II and III bursts must be able to explain the production of suprathermal and highly energetic electrons, since solar radio burst emission arises from such particles. Holman & Pesses [54] argued that these electrons are produced by shock drift acceleration, i.e., the electrons gain energy by reflection at the moving shock front. The increase in velocity can be calculated by

$$V_{\mathrm{f},\parallel} = 2v_{\mathrm{s}} \sec\phi - V_{\mathrm{i},\parallel}, \tag{101}$$

where is v_{s} the shock speed, ϕ the angle between the shock normal and the upstream magnetic field and $V_{\mathrm{f},\parallel}$ and $V_{\mathrm{i},\parallel}$ the particle velocity parallel to the magnetic field after and before the reflection, respectively. Assuming $T = 2 \times 10^6$ K for the solar corona gives the thermal speed of the electrons

$$v_{\mathrm{th,e}} = \sqrt{kT/m_{\mathrm{e}}} = 5500\,\mathrm{km\ s^{-1}}. \tag{102}$$

The "backbone" emission requires suprathermal electrons at $V_{\mathrm{f},\parallel} > 3\,v_{\mathrm{th,e}}$. Using

$$V_{\mathrm{i},\parallel} = \sqrt{2}\,v_{\mathrm{th,e}} = 7800\,\mathrm{km\ s^{-1}} \tag{103}$$

and $v_{\mathrm{s}} = 730\,\mathrm{km\ s^{-1}}$ leads to a validity limitation for $\phi \geq 80°$. Here I assumed that $V_{\mathrm{i},\parallel}$ can be expressed by the velocity of the greatest probability in a Maxwellian plasma, i.e., $V_{\mathrm{i},\parallel} = \sqrt{2}\,v_{\mathrm{th,e}}$.

For the "herringbone" emission, electrons with $V_{\mathrm{f},\parallel} = 78000\,\mathrm{km\ s^{-1}}$ are required. Assuming

$$V_{\mathrm{i},\parallel} = 2 \times \sqrt{2}\,v_{\mathrm{th,e}} = 15500\,\mathrm{km\ s^{-1}} \tag{104}$$

leads to the fact that these electrons can only be generated for $\phi \geq 88.5°$. Hence, shock drift acceleration may play a considerable role only for quasi-perpendicular shocks.

The energy gain for an electron after one reflection can be calculated by [102]

$$\frac{\epsilon_{\mathrm{f}}}{\epsilon_{\mathrm{i}}} = 1 + 4\left(\frac{B_2}{B_1} - 1\right). \tag{105}$$

For a coronal flare shock one can estimate the Alfvén Mach number with $M_A \simeq 1.5$, which gives an energy gain of about $\epsilon_{\mathrm{f}}/\epsilon_{\mathrm{i}} \simeq 3.5$.

4.1.2 SLAMS

In 1994 Mann & Lühr [75] proposed a mechanism responsible for electron acceleration at quasi-parallel shocks: So-called *SLAMS* (short large-amplitude magnetic field structures) were observed during in-situ measurements in the quasi-parallel region of Earth's bow shock [94]. Within SLAMS the magnetic field is deformed and changed into a quasi-perpendicular geometry and thus, electrons can be locally accelerated to high energies via shock drift acceleration, see Chapter 4.1.1. Mann & Lühr proposed that SLAMS exist also in the solar corona. Since SLAMS present strong magnetic enhancements, this could explain the multiple-lane fine structure often observed in solar type II bursts. Klassen et al. [60] showed an example of a type II burst created by a quasi-parallel shock.

4.1.3 Diffusive shock acceleration

The main idea behind this mechanism is that scattering permits a fast particle to bounce back and forth across a shock front many times. Thus, it gains energy by each reflection. The mechanism was suggested simultaneously by several authors in 1977-78, see Blandford [16], for example, and was applied to cosmic rays in the heliosphere and further astrophysical processes.

4.1.4 Stochastic acceleration

Stochastic acceleration, also called "Fermi acceleration", causes suprathermal electrons and ions to diffuse further to higher energies. This is due to random electric fields, as in MHD turbulences, structured electric fields, as in electrostatic double layers, or random particle motion. This acceleration mechanism can be described by a momentum diffusion coefficient $D(p)$. In general,

$$D(p) = \frac{\alpha p^2}{3\beta}, \tag{106}$$

where $v = c\beta$ is the particle speed and α the acceleration efficiency. See Miller et al. [82] and Park et al. [85] for an extensive description.

4.2 Emission processes

Since both type II and III emissions are due to plasma radiation emission, one can simultaneously treat both types. This includes the excitation of plasma waves by an agent, i.e., electrons running away from the shock front for type II and electron beams for type III bursts. The plasma waves finally transform into escaping electromagnetic waves by scattering off low-frequency structures or modes.

4.2.1 Emission at the fundamental plasma frequency

The emission at the fundamental plasma frequency arises from the non-linear interaction of a Langmuir wave L with an ion sound wave S which leads to an

escaping transverse electromagnetic wave T

$$L + S \rightarrow T. \tag{107}$$

Since

$$\omega_{\mathrm{L}} + \omega_{\mathrm{S}} = \omega_{\mathrm{T}} \tag{108}$$

and $\omega_{\mathrm{S}} \ll \omega_{\mathrm{L}}$ must be valid, process (107) leads to radio emission slightly above the local plasma frequency $\omega_{\mathrm{T}} \simeq \omega_{\mathrm{L}}$, where

$$\omega_{\mathrm{L}} \approx \omega_{\mathrm{p}}(1 + \frac{3}{2}k^2\lambda_{\mathrm{D}}^2) \tag{109}$$

with λ_{D} the Debye length. Furthermore, momentum conservation

$$\mathbf{k}_{\mathrm{L}} + \mathbf{k}_{\mathrm{S}} = \mathbf{k}_{\mathrm{T}} \tag{110}$$

must be fulfilled.

4.2.2 Emission at the second harmonic plasma frequency

The origin of the second harmonic is well accepted as being the result of the coalescence of two Langmuir waves

$$L_1 + L_2 \rightarrow T_{2\mathrm{L}}. \tag{111}$$

The conservation laws

$$\omega_1 + \omega_2 = \omega_{2\mathrm{L}} \simeq 2\omega_{\mathrm{L}}, \tag{112}$$

$$\mathbf{k}_1 + \mathbf{k}_2 = \mathbf{k}_{2\mathrm{L}} \tag{113}$$

must be fulfilled. This process is optically thin [120] and thus, $T_{2\mathrm{L}} \ll T_1$. According to Zheleznyakov [118], the brightness temperature of the radiation at the second harmonic can be calculated by

$$T_{2\mathrm{L}} \simeq \frac{8\pi^2}{15\sqrt{3}} \frac{\kappa e^2 f_{\mathrm{L}}^2 T_1^2 L_{2\mathrm{L}}}{m_{\mathrm{e}}^2 c^3 v_{\mathrm{T}}^2 v_{\mathrm{ph}}}, \tag{114}$$

where $f_{\mathrm{L}} = \omega_{\mathrm{L}}/2\pi$ is the local plasma frequency, κ Boltzmann's constant, $v_{\mathrm{T}} = \sqrt{\kappa T/m_{\mathrm{e}}}$ the thermal electron velocity, T_1 the brightness temperature of the Langmuir wave and $L_{2\mathrm{L}}$ the characteristic size of the region in which Langmuir waves with f_1 exist. From

$$\omega_1^2 = \omega_{\mathrm{L}}^2 + 3k_1^2 v_{\mathrm{T}}^2 \tag{115}$$

one can estimate $L_{2\mathrm{L}}$ as

$$L_{2\mathrm{L}} \simeq \frac{6k_1^2 v_{\mathrm{T}}^2}{\omega_{\mathrm{L}}^2} L_{\mathrm{N}}, \tag{116}$$

since

$$L_{\mathrm{N}} = N\left(\frac{dN}{dl}\right)^{-1}. \tag{117}$$

Setting $k_1 \simeq \omega_{\rm L}/v_{\rm ph}$ and inserting Eq. (116) into Eq. (114), one obtains

$$T_{2\rm L} \simeq \frac{4(2\pi)^2}{5\sqrt{3}} \frac{e^2\kappa}{m_{\rm e}^2 c^3} \frac{f_{\rm L}^2}{v_{\rm ph}^3} T_1^2 L_{\rm N}. \tag{118}$$

This expression for $T_{2\rm L}$ holds only for an isotropic spectrum of plasma waves and optically thin combinational scattering. In the anisotropic case, Eq. (114) contains a multiplier $\Psi(\theta) = \sin^2\theta\cos^2\theta$, where θ is the angle between $\mathbf{k}_1$ and $\mathbf{k}_{2\rm L}$. Momentum conservation implies an upper limit on the phase velocity of Langmuir waves participating in process (111):

$$v_{\rm ph} < \frac{2c}{\sqrt{3}}. \tag{119}$$

4.2.3 Emission at the third harmonic plasma frequency

The emission process for the third harmonic is most controversial. Since the third harmonic is observed quite rarely and has an unclear appearance, no theory could be tested satisfactorily.

The first possibility allowed by conservation laws is the two-step process

$$L_1 + L_2 \rightarrow T_{2\rm L}; \quad T_{2\rm L} + L_3 \rightarrow T_{3\rm L}. \tag{120}$$

The second possibility is the direct interaction of three Langmuir waves

$$L_1 + L_2 + L_3 \rightarrow T_{3\rm L}. \tag{121}$$

Zheleznyakov & Zlotnik [119] showed that process (120) is most probably responsible for the third harmonic emission in type III bursts, since process (121) has a smaller efficiency in the source of these bursts. On the other hand, the plasma waves involved in the second process of (120) need to fulfil the condition [22, 23, 119]

$$0.22c = \frac{c}{2\sqrt{2}+\sqrt{3}} < v_{\rm ph} < \frac{c}{2\sqrt{2}-\sqrt{3}} = 0.9c. \tag{122}$$

How does this inequality apply for type II and III emission? Since the origin of the "backbone" type II emission is unknown, one cannot make any statement about the validity of Eq. (122). The "herringbone" type II emission is believed to arise from electrons with $v_{\rm e} \sim 0.04\,c$. Since $v_{\rm e} \propto v_{\rm ph}$, one concludes that process (120) can not generate the third harmonic in "herringbones". However, Eq. (122) represents no restriction on the electrons generating type III bursts ($0.2c \leq v_{\rm e} \leq 0.6c$). Besides that, process (121) is not restricted by any conservation laws and may thus lead to generation of the third harmonic in both type II and III bursts.

According to Melrose [78], Tsytovich [103] and Zheleznyakov [117], the emissivity into the wave $T_{3\rm L}$ can be calculated as

$$a_{3\rm L}^{\omega} = \frac{k_{3\rm L}^2}{v_{3\rm L}^{\rm gr}} \frac{dW_{\mathbf{k}_{3\rm L}}}{dt}, \tag{123}$$

where

$$k_{3\mathrm{L}} = 2\sqrt{2}\frac{\omega_{\mathrm{L}}}{c}, \tag{124}$$

$$v_{3\mathrm{L}}^{\mathrm{gr}} = \frac{2\sqrt{2}}{3}c \tag{125}$$

and

$$\frac{dW_{\mathbf{k}_{3\mathrm{L}}}}{dt} = \int \Pi(\mathbf{k}_{3\mathrm{L}}, \mathbf{k}_1, \mathbf{k}_2, \mathbf{k}_3) W_{\mathbf{k}_1} W_{\mathbf{k}_2} W_{\mathbf{k}_3} d\Lambda \tag{126}$$

with

$$d\Lambda = \delta(\omega_{3\mathrm{L}} - \omega_1 - \omega_2 - \omega_3)\, \delta(\mathbf{k}_{3\mathrm{L}} - \mathbf{k}_1 - \mathbf{k}_2 - \mathbf{k}_3)\, d\mathbf{k}_1 d\mathbf{k}_2 d\mathbf{k}_3. \tag{127}$$

One can write the energy densities in terms of brightness temperatures of the plasma waves:

$$W_{\mathbf{k}_i} = \frac{\kappa T_i}{(2\pi)^3}. \tag{128}$$

Furthermore, we have

$$\Pi(\mathbf{k}_{3\mathrm{L}}, \mathbf{k}_1, \mathbf{k}_2, \mathbf{k}_3) = \frac{8\pi^2 \omega_{3\mathrm{L}}}{\partial(\omega_{3\mathrm{L}}^2 \epsilon_\perp)/\partial\omega_{3\mathrm{L}}} \frac{(4\pi)^3 \omega_1 \omega_2 \omega_3 |\mathbf{S}|^2}{|\partial\epsilon_\parallel/\partial\omega_1||\partial\epsilon_\parallel/\partial\omega_2||\partial\epsilon_\parallel/\partial\omega_3|}, \tag{129}$$

where $\mathbf{S}$ is the non-linear conductivity vector. I omit the very space consuming expression for $\mathbf{S}$ [120, Eq. (19)].

Let us assume an isotropic plasma. In this case we have

$$\epsilon_\parallel = 1 - \frac{\omega_{\mathrm{L}}^2}{\omega^2} \tag{130}$$

and

$$\epsilon_\perp = k^2 \frac{c^2}{\omega^2}. \tag{131}$$

Using Eqs. (130) and (131), one can calculate the denominator in Eq. (129). Assuming an isotropic Langmuir wave spectrum one may integrate Eq. (126):

$$\frac{dW_{\mathbf{k}_{3\mathrm{L}}}}{dt} \simeq \frac{2^9\pi^7}{3} \frac{\omega_{\mathrm{L}} k_1^3 \Delta k_1}{v_{\mathrm{T}}^2} W_{\mathbf{k}_1}^3 |\mathbf{S}|^2. \tag{132}$$

A simplified expression for $|\mathbf{S}|$ is [120, Eq. (21)]:

$$|\mathbf{S}| \simeq \frac{1}{16\pi} \frac{e^2}{m_{\mathrm{e}}^2} \frac{k_1^2}{\omega_{\mathrm{L}}^3}. \tag{133}$$

Thus, Eq. (126) may be simplified to

$$\frac{dW_{\mathbf{k}_{3\mathrm{L}}}}{dt} \simeq \frac{2\pi^5}{3} \left(\frac{e}{m_{\mathrm{e}}}\right)^4 \frac{k_1^7 \Delta k_1}{v_{\mathrm{T}}^2 c^3 \omega_{\mathrm{L}}^3} W_{\mathbf{k}_1}^3. \tag{134}$$

Now one can express the emissivity $a^{\omega}_{3\mathrm{L}}$ in terms of the brightness temperature of the Langmuir waves:

$$a^{\omega}_{3\mathrm{L}} \simeq \frac{\sqrt{2}}{8(2\pi)^4}\left(\frac{e}{m_\mathrm{e}}\right)^4 \frac{k_1^7 \Delta k_1 \kappa^3}{v_\mathrm{T}^2 c^3 \omega_\mathrm{L}^3} T_1^3. \tag{135}$$

For the optical thin case the brightness temperature of the third harmonic may be expressed as:

$$T_{3\mathrm{L}} = \frac{\pi c^2}{f_{3\mathrm{L}}^2 \kappa} a^{\omega}_{3\mathrm{L}} L_{3\mathrm{L}}. \tag{136}$$

One may assume $L_{3\mathrm{L}} \simeq L_{2\mathrm{L}}$ [7] and thus rewrite Eq. (136) as

$$T_{3\mathrm{L}} \simeq \frac{\sqrt{2}\pi^2}{6}\frac{\kappa^2}{c}\left(\frac{e}{m_\mathrm{e}}\right)^4 \frac{f_\mathrm{L}^3}{v_\mathrm{ph}^{10}} T_1^3 L_\mathrm{N}. \tag{137}$$

Logically, we have $T_{3\mathrm{L}} \simeq T_1^3$, i.e., the brightness temperature of the third harmonic $T_{3\mathrm{L}}$ is the third power of that of the Langmuir wave T_1. Furthermore, $T_{3\mathrm{L}}$ is strongly dependent on v_ph ($T_{3\mathrm{L}} \propto v_\mathrm{ph}^{10}$).

To avoid aforementioned difficulties with process (121), Cairns [22, 23] suggested the following three-step process

$$L + S \to L'; \quad L'_1 + L'_2 \to T_{2\mathrm{L}}; \quad T_{2\mathrm{L}} + L' \to T_{3\mathrm{L}} \tag{138}$$

for explaining multiple plasma radiation in Earth's bow shock. Kliem [64] transferred typical plasma parameters for solar type II bursts to explain their harmonic radiation. Process (138) is of importance only if the transformation of Langmuir waves into Langmuir waves with greater phase velocity is optically thick,[6] i.e., the energy density of the "fast" Langmuir waves is not less than the energy density of the "slow" Langmuir waves. Furthermore, ion-sound waves occur only in non-isothermal plasmas, i.e., $T_\mathrm{e} \neq T_\mathrm{i}$. However, in the solar corona, which contains the source of solar radio burst emission, we rather need to consider thermodynamic equilibrium. An appropriate process in isothermal plasmas that replaces the first step in process (138) may be induced scattering of Langmuir waves on ions:

$$L_1 \to L' + I. \tag{139}$$

Note that the L'-waves need to fulfil inequality (122). Zaitsev [114, 115] estimated the efficiency of process (139) assuming that the initial width of the k_1-spectrum of the plasma waves is larger than the change of k_1 during one interaction. Thus, the change of the averaged spectral density $W_{\mathrm{k}_1} = k_1^2 W_{\mathbf{k}_1}$ can be calculated by [58]

$$\frac{\partial W_{\mathrm{k}_1}}{\partial t} = \alpha^1 W_{\mathrm{k}_1} \frac{\partial W_{\mathrm{k}_1}}{\partial k_1}, \tag{140}$$

[6] See also Chapter 2.1.

where the probability $\alpha^{\rm l}$ is

$$\alpha^{\rm l} = \frac{4\pi}{27} \frac{e^2 \omega_{\rm L}}{m_{\rm e} m_{\rm i} v_{\rm T}^4 (1 + T_{\rm e}/T_{\rm i})^2}. \tag{141}$$

The typical time scale of change of $W_{\rm k_1}$ is then

$$\gamma_1 = \frac{1}{W_{\rm k_1}} \frac{\partial W_{\rm k_1}}{\partial k_1} \sim \alpha^{\rm l} \frac{\partial W_{\rm k_1}}{\partial k_1}. \tag{142}$$

Thus, the coefficient of spatial decay or growth is given by

$$\mu_1 = \frac{\gamma_1}{v_1^{\rm gr}} = \frac{\alpha^{\rm l}}{v_1^{\rm gr}} \frac{\partial W_{\rm k_1}}{\partial k_1}. \tag{143}$$

Using Eq. (143), one can transform Eq. (9) for the optical depth into

$$\tau_1 = \int \mu_1 \, dl = \int \frac{\alpha^{\rm l}}{v_1^{\rm gr}} \frac{\partial W_{\rm k_1}}{\partial k_1} dl. \tag{144}$$

One may replace the integration over the ray path dl in Eq. (144) by integration over wave numbers k_1, since

$$dl = \frac{6 L_{\rm N} k_1 v_{\rm T}^2}{\omega_{\rm L}^2} dk_1, \tag{145}$$

which follows from

$$\omega_1^2 = \omega_{\rm L}^2(l) + 3 k_1^2(l) v_{\rm T}^2 = const. \tag{146}$$

Using Eq. (141) and $v_1^{\rm gr} = 3 k_1 v_{\rm T}^2 / \omega_{\rm L}$, one can rewrite Eq. (144) as follows:

$$\tau_1 = \frac{8\pi^2}{27} \frac{e^2 L_{\rm N}}{m_{\rm e} m_{\rm i} v_{\rm T}^4 (1 + T_{\rm e}/T_{\rm i})^2} \int \frac{\partial W_{\rm k_1}}{\partial k_1} dk_1. \tag{147}$$

The integral in Eq. (147) may be considered as some averaged value $W_{\rm k_1}$ and can thus be approximated by

$$W_{\rm k_1} = \frac{k_1^2 \kappa T_1}{(2\pi)^3}. \tag{148}$$

Hence, we finally obtain the optical depth

$$\tau_1 = \frac{4\pi}{27} \frac{e^2 \kappa}{m_{\rm e} m_{\rm i} v_{\rm T}^4 (1 + T_{\rm e}/T_{\rm i})^2} \frac{f_{\rm L}^2 T_1^2 L_{\rm N}}{\alpha^2}, \tag{149}$$

where

$$\alpha = \frac{v_{\rm ph}}{v_{\rm T}}. \tag{150}$$

Thus, for $f_{\rm L} \simeq 160\,{\rm MHz}$, $v_{\rm T} = 3 \times 10^5$ m/s and an inhomogeneity density scale length $L_{\rm N} \sim 10^6$ m, Eq. (149) gives

$$\tau_1 \sim 9 \times 10^{-11} \frac{T_1}{\alpha^2}. \tag{151}$$

Induced scattering (139) is efficient only if the process is optically thick, i.e., $\tau_1 > 1$. At $\alpha \sim 3$ (for $v_{\rm ph} \sim 10^6\,{\rm m/s}$), this inequality holds only if the brightness temperature of the "slow" Langmuir waves fulfils

$$T_1 > 10^{10}\ {\rm K}. \tag{152}$$

Condition (152) is fulfilled in type II sources. Hence, Langmuir waves with smaller phase velocity may in fact be transformed into waves with greater phase velocity, which are necessary for the second step in process (138). Thus, one may summarize that the radiation at the third harmonic plasma emission in type II bursts is due a modification of process (138):

$$L_1 \to L' + I; \quad L_1' + L_2' \to T_{2L}; \quad T_{2L} + L' \to T_{3L}. \tag{153}$$

The emissivity of the electromagnetic waves resulting from process (153) can be calculated as follows [103]:

$$\begin{aligned} w^{\rm t}_{\rm t,l'}({\bf k}_{\rm 3L}, {\bf k}_{\rm 2L}, {\bf k}') =& \frac{\hbar e^2 (2\pi)^6 \omega_L (k')^2}{16\pi m_{\rm e}^2 \omega_{\rm 3L}({\bf k}_{\rm 3L})\omega_{\rm 2L}({\bf k}_{\rm 2L})} \left(1 + \frac{({\bf k}_{\rm 2L}{\bf k}_{\rm 3L})^2}{k_{\rm 2L}^2 k_{\rm 3L}^2}\right) \\ & \times \delta({\bf k}_{\rm 3L} - {\bf k}_{\rm 2L} - {\bf k}')\delta(\omega_{\rm 3L} - \omega_{\rm 2L} - \omega'), \end{aligned} \tag{154}$$

where $w^{\rm t}_{\rm t,l'}$ is the probability of coalescence of plasma and electromagnetic waves into electromagnetic waves. Using Eq. (128), one can transform the transfer equation for the energy density [117, 118]

$$\frac{dW_{\rm k_{3L}}}{dt} = \int w^{\rm t}_{\rm t,l'} \frac{\omega_{\rm 3L}}{\omega_{\rm 2L}\omega'} W_{\rm k_{2L}} W_{\rm k'} \frac{d{\bf k}_{\rm 2L} d{\bf k}'}{\hbar(2\pi)^3} \tag{155}$$

into

$$\frac{dT_{\rm 3L}}{dt} \simeq \frac{3\kappa}{2\hbar\omega_{\rm L}} \int w^{\rm t}_{\rm t,l'}({\bf k}_{\rm 3L}, {\bf k}_{\rm 2L}, {\bf k}') T' T_{\rm 2L} \frac{d{\bf k}_{\rm 2L} d{\bf k}'}{(2\pi)^6}. \tag{156}$$

Integration over $d{\bf k}_{\rm 2L}$ leads to

$$\frac{dT_{\rm 3L}}{dt} \simeq \frac{\kappa e^2}{32\pi m_{\rm e}^2 \omega_{\rm L}^2} \int T' T_{\rm 2L} \delta(\omega_{\rm 3L} - \omega_{\rm 2L} - \omega')(k')^2 d{\bf k}', \tag{157}$$

where I assumed

$$\frac{({\bf k}_{\rm 2L}, {\bf k}_{\rm 3L})^2}{k_{\rm 2L}^2 k_{\rm 3L}^2} \sim 1. \tag{158}$$

Note that

$$d{\bf k}' = (k')^2 \sin\theta d\varphi d\theta dk' \tag{159}$$

and

$$k_{\rm 2L}^2 = ({\bf k}_{\rm 3L} + {\bf k}')^2 = k_{\rm 3L}^2 - (k')^2 - 2k_{\rm 3L}k'\cos\theta. \tag{160}$$

Integration over $d\theta$ by using $\delta(\omega_{\rm 3L} - \omega_{\rm 2L} - \omega')$ gives

$$\frac{\partial\omega_{\rm 2L}}{\partial\theta} = \frac{\partial\omega_{\rm 2L}}{\partial k_{\rm 2L}^2} 2k_{\rm 3L}k'\sin\theta = \sqrt{2}k'c\sin\theta \tag{161}$$

Time UT	Freq. MHz	Band	T_b^{max} [10^9K]	Source size [']	[HPBW]	Flux [10^4 Jy]
			27 Sep 1993			
12:10:57-	164	f_L	3.5	3.7	3.1	280
-12:11:14	327	$2f_L$	85	1.9	1.6	7100
	435	$3f_L$	0.7	1.6	1.8	73
12:11:20-	236	$2f_L$	380	2.3	2.7	22000
-12:11:40	327	$3f_L$	0.3	1.8	1.5	20
12:12:00-	236	$2f_L$	300	2.4	2.9	21000
-12:12:35	327	$3f_L$	0.9	2.0	1.7	82
			28 Dec 1993			
12:12:07	236	$2f_L$	0.9	2.2	2.7	47
12:12:37	327	$3f_L$	0.3	1.5	1.3	14
12:13:22	164	$2f_L$	1.6	2.3	1.9	46

Table 1: Brightness temperature of the fundamental and harmonics of type II bursts. OSRA. 1 Jy = 10^{-26} $Wm^{-2}Hz^{-1}$. HPBW: half-power bandwidth. Adapted from Zlotnik et al. [120, Table 1].

in the denominator in Eq. (157). Thus, integration over $d\mathbf{k}'$ gives

$$\frac{dT_{3L}}{dt} = \frac{1}{16\sqrt{2}} \frac{\kappa e^2}{m_e^2 c \omega_L^2} \int (k')^3 T' T_{2L} dk'. \tag{162}$$

The integration limits are given by Eq. (122), i.e.,

$$1.1 \frac{\omega_L}{c} \leq k' \leq 4.5 \frac{\omega_L}{c}. \tag{163}$$

Let us approximate

$$\int (k')^3 T' T_{2L} dk' \sim (k')^3 T' T_{2L} \Delta k', \tag{164}$$

since the exact dependence on k' is unknown. Furthermore, I put

$$k' = a \frac{\omega_L}{c} \tag{165}$$

with $1.1 \leq a \leq 4.5$ and assume $\Delta k' \sim k'$. Thus, Eq. (162) may be simplified to

$$\frac{dT_{3L}}{dt} \sim \frac{\pi a^2}{4\sqrt{2}} \frac{\kappa e^2}{m_e^2 c^5} f_L^2 T' T_{2L}. \tag{166}$$

Using Eqs. (123) and (136), we get

$$T_{3L} \simeq \frac{\sqrt{2}}{3c} \frac{dT_{3L}}{dt} L_{3L}. \tag{167}$$

Here, one needs to assume that $L_{3\mathrm{L}} \sim L_{\mathrm{N}}$, unlike for process (121). This is due to the fact that the spectrum of the second harmonic originates from all elements of the nonuniform source [119]. This leads to

$$T_{3\mathrm{L}} \simeq \frac{\pi^2 a^4}{12} \frac{\kappa e^2}{m_{\mathrm{e}}^2 c^6} f_{\mathrm{L}}^2 T' T_{2\mathrm{L}} L_{\mathrm{N}}. \tag{168}$$

One may replace $T_{2\mathrm{L}}$ by Eq. (118) and approximate T' by $T' \sim T_1$, since T' can only be obtained by a self-consistent analysis of the plasma wave transfer across the spectrum. Finally one obtains:

$$T_{3\mathrm{L}} \sim \frac{4\pi^4 a^4}{15\sqrt{3}} \frac{\kappa^2 e^4}{m_{\mathrm{e}}^4 c^9} \frac{f_{\mathrm{L}}^4 T_1^3 L_{\mathrm{N}}^2}{v_{\mathrm{ph}}^3}. \tag{169}$$

Note that v_{ph} is the phase velocity of the "slow" Langmuir waves creating the second harmonic, not of the "fast" Langmuir waves generating the third harmonic.

4.3 Collisionless Shocks

Type II bursts are thought to arise from fast magnetosonic shocks [77, Ch. 13]. Here a short outline of important characteristics of collisionless shocks is given.

Up- and downstream quantities of a shock wave are related by the Rankine-Hugoniot relations, see Priest [89] for an overview. For an oblique shock one obtains

$$\begin{aligned} &M_{\mathrm{A}1}^2 X \sin^2\theta \left[\left\{ \gamma + X(2-\gamma) \right\} M_{\mathrm{A}1}^2 - X \left\{ (\gamma+1) - X(\gamma-1) \right\} \right] \\ &+ (M_{\mathrm{A}1}^2 - X)^2 \left[\gamma \beta_1 X + M_{\mathrm{A}1}^2 \cos^2\theta \left\{ X(\gamma-1) - (\gamma+1) \right\} \right] = 0, \end{aligned} \tag{170}$$

where $M_{\mathrm{A}1}^2 = v_1 / v_{\mathrm{A}1}$ the Alfvén-Mach number, $X = N_2/N_1$ the density jump across the shock and θ the angle between the shock normal $\mathbf{n}_{\mathrm{s}}$ and the upstream magnetic field $\mathbf{B}_1$. The indices 1 and 2 describe the quantities in the up- and downstream region, respectively. Furthermore, the Alfvén velocity is given by

$$v_{\mathrm{A}1} = \frac{B_1}{\sqrt{\mu_0 m_{\mathrm{p}} N_1}} \tag{171}$$

and the upstream plasma beta is obtained from

$$\beta_1 = \frac{2\mu_0 N_1 k_{\mathrm{B}} T_1}{B_1^2}. \tag{172}$$

Thus, the increase of the magnetic field can be calculated by

$$\left| \frac{B_2}{B_1} \right| = \sqrt{\cos^2\theta + \left(\frac{M_{\mathrm{A}1}^2 - 1}{M_{\mathrm{A}1}^2 - X} \right) X^2 \sin^2\theta}. \tag{173}$$

Usually the three solutions to Eq. (170) refer to fast, intermediate and slow shocks, respectively.

A fast magnetosonic shock is critical if $v_{n2} = c_{s2}$, i.e., if the downstream speed parallel to the shock normal v_{n2} equals the downstream sound speed c_{2s} given by

$$c_{2s} = \sqrt{\frac{\gamma p_2}{\rho_2}} \tag{174}$$

with ρ_2 the mass density in the downstream region. Thus, M_{A1} may be replaced by the critical Alfvén Mach number M_{A1}^{crit} such that Eq. (170) transforms into

$$\begin{aligned}&(M_{A1}^{crit} - X)^2 \Big\{(\gamma+1)(M_{A1}^{crit})^2 \cos^2\theta - \gamma\beta_1 X^2 - (M_{A1}^{crit})^2 X^2\Big\} \\ &+ (\gamma-1)(M_{A1}^{crit})^2 X^2 \Big\{(M_{A1}^{crit})^2 - 1\Big\}^2 \sin^2\theta = 0.\end{aligned} \tag{175}$$

Thus, one may calculate M_{A1}^{crit}, according to Mann et al. [73] $1.2 \leq M_{A1}^{crit} \leq 2.3$ for quasi-parallel shocks and $1.5 \leq M_{A1}^{crit} \leq 2.8$ for quasi-perpendicular shocks. Furthermore, they assumed that the relative instantaneous bandwidth is related to the density jump accross the shock

$$\frac{\Delta f}{f} = \frac{f_{p2} - f_{p1}}{f_{p1}} = \sqrt{\frac{N_2}{N_1}} - 1 = \sqrt{X} - 1. \tag{176}$$

In a statistical analysis of type II bursts they found a smallest value for the instantaneous bandwidth ($\Delta f/f = 0.16$) which corresponds to a density jump of $X = 1.35$. Thus, one may conclude that the type II exciter must exceed a threshold in order to generate type II emission. This agrees quite well with observations, since not every flare or CME is accompanied by a type II burst. Let me point out that there are several theories on the source location of type II bursts. Lampe & Papadopoulos [70] and Krall & Smith [65] assumed downstream emission while Holman & Pesses [54], Krasnosel'skikh et al. [66] and Benz & Thejappa [13] favoured upstream emission. Early theories considered even the transition region of the shock to be the locus of the emission. Recent in-situ observations by Hoang et al. [53] showed that fundamental and harmonic emission originates from the down- and upstream region, respectively. The ALFA mission could provide a unique possibility to prove these theories. See Chapter 5.1 for further details.

5 Low frequency radio astronomy from space and solar radio bursts

5.1 The Astronomical Low Frequency Array (ALFA)

The frequency window between 30 kHz (just above the interplanetary plasma frequency) and 30 MHz (a few times the plasma frequency in the ionosphere of the Earth) is the last unexplored part of the electromagnetic spectrum. Ground based radio telescopes may observe down to 10 MHz on the nightside near sunspot minimum and down to 15 MHz on the dayside near sunspot maximum. Near special locations on Earth, i.e., near the magnetic poles, measurements down to 2 MHz were performed. This resulted in quite poor resolution: Galactic surveys were obtained with the Llanherne array in Tasmania with a resolution of about 5.6° at 3.7 MHz [24] and 2.6° at 8 MHz [26]. Note that radiation from within our Galaxy may be not be received below $\sim$ 1 MHz due to the high absorption coefficient of the interstellar ionized hydrogen at lower frequencies [1].

The Astronomical Low Frequency Array (ALFA),[7] proposed by the JPL and NRL, will provide the first sensitive, high-angular resolution radio survey at low frequencies and thus open a new window for astronomical investigations. Figure 15 shows ALFA's angular resolution vs. frequency compared with existing ground-based radio observatories. It will consist of 16 small satellites, each equipped with crossed dipole antennas. The satellites will be placed in a spherical array with a diameter of about 100 km in a distant (10^6 km), interference-free and stable orbit around the Earth. Terrestrial interference will not be a problem for ALFA. Measurements by the WAVES instrument on the WIND spacecraft showed that above 6 MHz 93% of the observations are within 3% of the galactic background, see Figure 16. Taylor et al. [100] investigated the propagation of terrestrial radio emissions through the ionosphere to analyze the low frequency radio noise environment for ALFA.

The scientific reward of this project can be expected to be rather great. Firstly, new unexpected phenomena may be discovered. Harwit [46] estimated in an interesting analysis that one third of the phenomena in the universe have been discovered. Of the 43 phenomena in his study, 39 can be found in a frequency range from 3 $\times 10^7$ MHz to 3×10^{15} MHz. So one just can guess how many unknown phenomena one may encounter in the frequency range from 30 kHz to 30 MHz observed by ALFA. Secondly, as Harwit stated, improved observing capabilities lead also to a great scientific return, as proved by other all-sky survey missions in spectral regions not observable from Earth, such as IRAS, Uhuru and GRO. In the following a short overview of the ALFA scientific objectives are given:

1. Solar radio bursts: Several solar phenomena such as flares, filament eruptions and CMEs manifest themselves in different non-thermal radio bursts. ALFA will provide highly resolved measurements, both temporally and spatially. Thus, one may be able to sense the solar and interplanetary

[7] ALFA homepage: http://sgra.jpl.nasa.gov/html_dj/ALFA.html

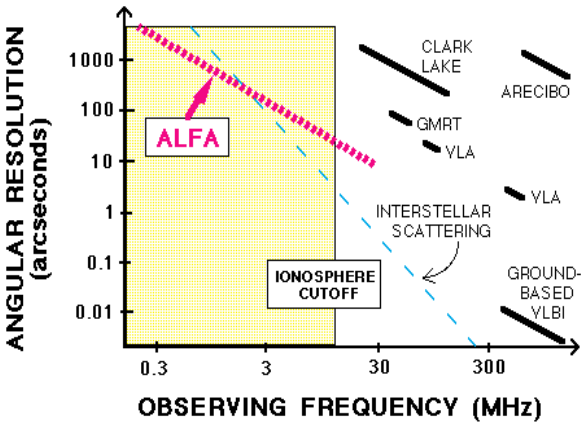

Figure 15: ALFA's angular resolution in comparison with other radio observatories. Taken from http://sgra.jpl.nasa.gov/html_dj/ALFA-res.gif.

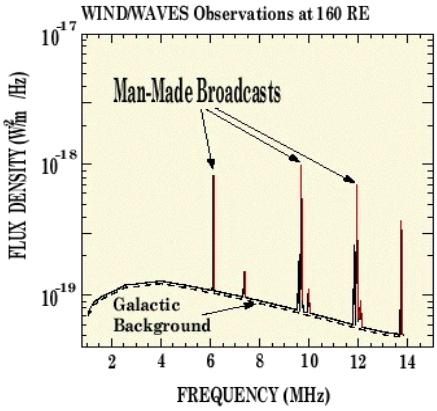

Figure 16: Observation of artificial interferences measured by WIND. Taken from http://sgra.jpl.nasa.gov/html_dj/ALFA-RFI.gif.

plasma density and magnetic field structures between the Sun and Earth. Furthermore, one may track solar disturbances from the Sun to the vicinity of the Earth. Earthbound measurements allow only tracking to ~ 30 MHz, i.e., a height above the Sun of about $\sim 0.5\,R_S$. This makes space-based radio observations absolutely urgent. Eventually, this may lead to improved heliospheric density models [74] which is essential for a better understanding of interplanetary space plasma and an improved space weather fore-

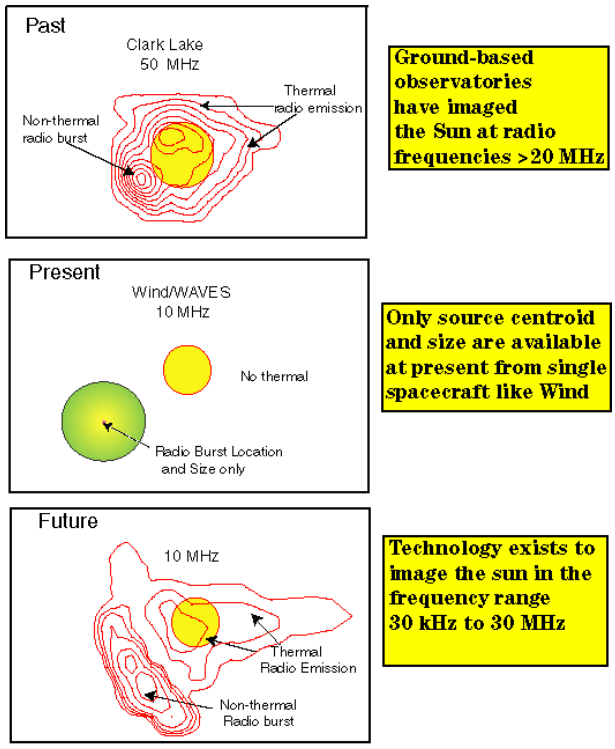

Figure 17: Progress in resolution gained by ALFA. Taken from http://sgra.jpl.nasa.gov/html_dj/ALFA-SEC.gif.

casting.

In fact, several spacecraft missions observing the Sun at low frequencies have been launched, such as the Radio Astronomy Explorer (RAE 1 and 2) [2, 106]. However, the measurements were obtained from single spacecraft with simple dipole antennas. Thus, one could track only the centroids of the radio type III bursts due to the poor angular resolution. As shown in Figure 17, the improvement in resolution and detection of both thermal and non-thermal emission is essential. The upper part of Figure 17 shows a superposition of solar thermal emission with non-thermal emission of a type III burst observed by Clark Lake at 50 MHz. The middle part of Figure 17 gives an impression of a measurement of the same bursts shown in the upper part obtained by the WAVES instrument on the WIND spacecraft. Here, only the centroid of the bursts can be observed, but no spatial resolution or detection of thermal radiation is achieved [76]. The lower part of Figure 17 shows the expected observation by ALFA. Both thermal and non-thermal emissions can be imaged simul-

taneously providing high temporal and spatial resolution. Furthermore, ALFA will track solar disturbances to distances of about 1 AU. Mapping of the vicinity of the shocks associated with type II bursts would provide further information on sites of particle acceleration. Finally, behind-the-limb type III bursts are scattered back and hence illuminate transient CMEs instantaneously due to their high speed. This would be helpful to map these transient phenomena.

2. The "quiet" Sun: Coronal holes and streamers are the main characteristics of the quiet Sun. The first are sources of the fast solar wind and the latter overlie dark filaments and resemble the pre-eruptive state of CMEs. The dominating emission of the quiet Sun is thermal bremsstrahlung from the corona ($T \sim 10^6$ K). Ground-based measurements were obtained down to the ionospheric cutoff. X-ray observations could follow the propagation of these disturbances to rather small distances from the Sun. ALFA will provide monitoring of these phenomena from the solar corona to distances far behind the orbit of the Earth. Especially Earth-directed CMEs, so-called Halo-CMEs, may be predicted more precisely.

3. Mapping of interplanetary density structures: By tracking type III bursts, which can propagate far behind the orbit of the Earth, one may obtain detailed maps of the interplanetary magnetic field. Since type III bursts are travelling along open field lines outward from the Sun, they directly reveal the field line structure. Furthermore, the magnetic field around CMEs will be provided. This is essential for the understanding of the role of CMEs in particle injection and/or acceleration for solar radio bursts. As mentioned before, the association between flares and CMEs is not clearly demonstrated, neither their importance during radio burst events.

4. Terrestrial impacts: The most geoeffective disturbances are the fast solar wind, exhibiting a 27-day-periodicity, prominence eruptions and CMEs. Geomagnetic storms constitute a considerable danger for Earth-based and space-borne technological systems and, of course, astronauts. ALFA will solve two of the greatest problems: The prediction of the arrival of such a disturbance and its geoeffectiveness. CMEs that are related with shocks are most geoeffective and may be tracked directly by observing the associated type II emission. Slower moving CMEs that do not produce shocks may be tracked directly by measuring the enhanced thermal bremsstrahlung or indirectly by using illumination by behind-the-limb type III bursts. Nowadays, solar coronographs predict Earth arrival within an error of a day or two. ALFA will improve the error to the range of hours.

   ALFA will also provide new insight into the Earth's magnetosphere. The Auroral Kilometric Radiation (AKR) is observed below a few hundred kHz and is an example of the Earth's natural radio emission. Furthermore, plasma emissions at twice the local plasma frequency is generated at the Earth's bow shock. Deeper within the magnetosphere the nightside AKR

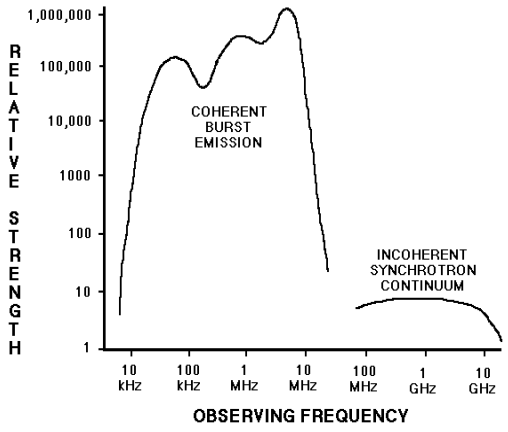

Figure 18: Time-averaged radio emission from Jupiter. Taken from http://sgra.jpl.nasa.gov/html_dj/ALFA-spectrum.gif.

is scattered off of dayside density irregularities which characterizes the day-side cusp. These structures will be observed, highly spatially and temporally resolved, by ALFA.

5. Evolution of galaxies: ALFA will also look for "fossil" galaxies to determine the frequency and duration of the active phase of galactic nuclei. This information on early epochs of galaxies could lead to an improvement of models for the evolution of massive black holes in galactic nuclei. Furthermore, ALFA could take a look back into the protogalaxy era by exploring higher redshifts which are typical for galaxies with steep spectra at low frequencies.

6. Life cycles of matter in the universe: The interstellar ionized hydrogen is the last major component of the interstellar medium whose distribution is not accurately known. However, the large-scale distribution is essential for our understanding of the interstellar extinction caused by this gas. Furthermore, ALFA could test the theory that cosmic rays are created in supernova remnants. This could be done by directly measuring low energy energy electrons needed for initiating shock acceleration. In addition, mapping of the 3D distribution of galactic low energy cosmic ray electrons could be helpful for further the progress in understanding cosmic ray propagation.

7. Testing of theories and discovery of new phenomena: Note that most of the processes participating in emission and absorption processes are only observable at low radio frequencies. Strong coherent emitting processes are common at low frequencies. Figure 18 shows the relative strength of

coherent and incoherent emission from Jupiter. This intense coherent radiation provides a wealth of information on the local plasma and is only observable at low frequencies. Similar coherent processes are expected from supernova remnants, quasars and active galaxies. Furthermore, ALFA will perform spectral measurements of supernova remnants, thus locating shock acceleration sites which are held responsible for the generation of high energy cosmic rays. Especially, ALFA will detect low energy electrons that are essential for injection processes in to shock acceleration mechanisms. This cannot be done by X-ray observations. Another interesting possibility provided by ALFA is the direct detection of coherent cyclotron radiation from extrasolar planets. Although the radiation originating from Jupiter is below the detection limit of ALFA, this limit might be exceed by other giant planets, since stellar-wind-driven cyclotron emission is strongly depended on the stellar wind flux. It is proved that in some stellar systems the stellar wind flux exceeds that of the Sun by many orders of magnitude.

ALFA was subject of two conferences [107, 110] and was also presented on more general meetings [57, 111]. Furthermore, a scientific article [109] and a public article [108] have been published. For a summarizing overview I suggest the report to the "Radio & Submm Astronomy Panel"[8] which outlines the scientific goals, objectives and needs for starting the Astronomical Low Frequency Array.

Unfortunately, no further progress concerning the initiation of the ALFA mission has been achieved since the last NASA call for MIDEX proposals a couple of years ago. A limitation to the observation of solar radio bursts is considered as a promising approach for the next proposal. Furthermore, the Nanny nano-satellite mission could provide evidence for the enormous possibilities hidden in such a mission.

5.2 The nano-satellite Nanny

The development of the nano-satellite Nanny started in 1998 at IRFU. The first phase concentrated on the development of miniaturised and more efficient components, sensors and subsystems in general. Nanny-1 can be considered as a modernised and miniaturised version of the Astrid-3 nano-satellite.

Some of the scientific objectives are the establishment of the relationship between space plasma turbulence and electromagnetic radiation. This would be an essential milestone to further our progress in space physics. Furthermore, extended studies of the interplay between the local self-organisation of the space plasma and the surrounding medium will be performed. In-situ studies of the Stimulated Electromagnetic Emission (SEE), a phenomenon discovered by Bo Thidé at IRFU, are of high interest also since this effect may limit the bandwidth of low-altitude satellite global telecommunication systems. In the same manner as ALFA, Nanny will track low-frequency solar radio bursts as well as

[8] http://rsd-www.nrl.navy.mil/7214/weiler/kwpdf/report-long6.pdf

the Auroral Kilometric Radiation (AKR) and other "natural" electromagnetic emissions by using new antenna, detector and signal techniques.

Nanny-1 is suggested to be followed by a pair of nano-satellites, Nanny-2 and Nanny-3. The use of such a "mini"-interferometer will drastically improve the spatial and temporal resolution. Thus, the Nanny project can be a convenient precursor mission to the Astronomical Low Frequency Array (ALFA).

At the moment, extensive Phase-A and Phase-B studies are performed in order to apply for fundings to build the first spacecraft. For more information I refer to the Nanny homepage[9] at IRFU, since no publication is available yet. It is planned to launch Nanny-1 in the end of 2002 or the beginning of 2003.

6 Acknowledgements

I want to thank my supervisor Bo Thidé for the opportunity to write my diploma thesis at the Swedish Institute of Space Physics, Uppsala division. Furthermore, I want to thank Gottfried Mann and Henry Aurass, Solar Radio Observatory (OSRA)[10] at the Astrophysical Institute Potsdam, for their extensive help by providing spectra of solar radio bursts. Special thanks to Henry Aurass for his very helpful comments about my thesis. Finally, I want to thank Dayton Jones, JPL, Pasadena, and Kurt W. Weiler, NRL, Washington, D.C., for very useful information concerning the ALFA mission.

[9]Nanny homepage: http://www.wavegroup.irfu.se/Nanny/index.html
[10]OSRA homepage: http://www.aip.de/groups/osra

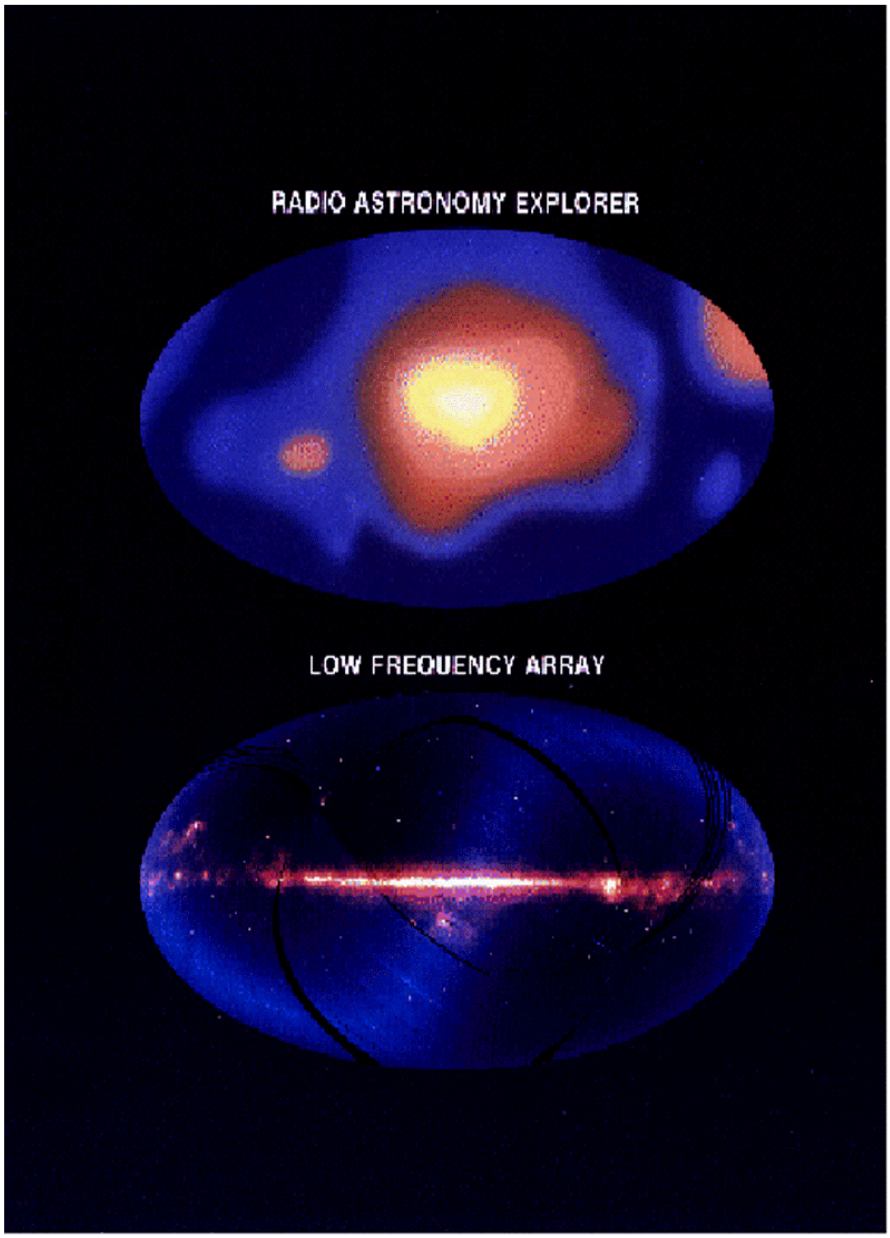

Figure 19: Comparison of all-sky surveys obtained by ALFA (simulated) and RAE. Taken from http://rsd-www.nrl.navy.mil/7214/weiler/kwgif/lfsky.gif.

References

[1] J.K. Alexander et al. The spectrum of the cosmic radio background between 0.4 and 6.5 MHz. *Ap. J. Lett.*, 157:L163–L165, 1969.

[2] J.K. Alexander and J.C. Novaco. Survey of the galactic background radiation at 3.93 and 6.55 MHz. *Astron. J.*, 79:777–785, 1974.

[3] S.K. Antiochos, C.R. DeVore, and J.A. Klimchuk. A model for solar coronal mass ejections. *Ap. J.*, 510:485–493, 1999.

[4] D. Arakawa. Abnormal attenuation in short radio wave propagation. *Rep. Radio Res. Japan*, 6:31–38, 1936.

[5] M.J. Aschwanden, A.O. Benz, and R.A. Schwartz. The timing of electron beam signatures in hard X-ray and radio: Solar flare observations by BATSE/COMPTON GAMMA-RAY OBSERVATORY and PHOENIX. *Ap. J.*, 417:790–804, 1993.

[6] M.J. Aschwanden et al. Solar electron beams detected in hard X-rays and radio waves. *Ap. J.*, 455:347–365, 1995.

[7] H. Aurass, A. Hofmann, and H.-W. Urbarz. The 09 September 1989 γ-ray flare: Multi-site particle acceleration and shock-excited radio emssion during quasiperpendicular and quasiparallel propagation. *Astron. Astrophys.*, 334:289–298, 1998.

[8] G. Bekefi. *Radiation processes in plasmas.* John Wiley & Sons, New York, 1966.

[9] A.O. Benz. Millisecond spike bursts. *Sol. Phys.*, 104:99–110, 1986.

[10] A.O. Benz. *Plasma astrophysics.* Kluwer Academic Publishers, Dordrecht, 1993.

[11] A.O. Benz et al. Electron beams in the low corona. *Sol. Phys.*, 141:335–346, 1992.

[12] A.O. Benz and G. Mann. Intermediate drift bursts and the coronal magnetic field. *Astron. Astrophys.*, 333:1034–1042, 1998.

[13] A.O. Benz and G. Thejappa. Radio emission of coronal shock waves. *Astron. Astrophys.*, 202:267–274, 1988.

[14] A.O. Benz and P. Zlobec. Correlation between drift rate and polarization in solar type III radio bursts. *Astron. Astrophys.*, 63:137–145, 1978.

[15] T. Bernold. A catalogue of fine structures in type IV solar radio bursts. *Astron. Astrophys. Suppl. Ser.*, 42:43–58, 1980.

[16] R.D. Blandford and J.P. Ostriker. Particle acceleration by astrophysical shocks. *Ap. J. Lett.*, 221:L29–L32, 1978.

[17] E. Böhm-Vitense. *Introduction to stellar astrophysics, Vol. 2: Stellar atmospheres.* Cambridge University Press, Cambridge, 1989.

[18] J.G. Bolton and G.J. Stanley. Variable source of radio frequency radiation in the constellation of Cygnus. *Nature*, 161:312–313, 1948.

[19] T.J.M. Boyd and J.J. Sanderson. *Plasma Dynamics.* Nelson & Sons, London, 1969.

[20] R.N. Bracewell, editor. *Paris symposium on radio astronomy*, volume 9 of *IAU Symp.* Stanford University Press, Stanford, 1959.

[21] B.F. Burke and K.L. Franklin. Observations of a variable radio source associated with the planet Jupiter. *J. Geophys. Res.*, 60:213–217, 1955.

[22] I.H. Cairns. Third and higher harmonic plasma emission due to raman scattering. *J. Plasma Phys.*, 38:199–208, 1987.

[23] I.H. Cairns. A theory for the radiation at the third to fifth harmonics of the plasma frequency upstream from the Earth's bowshock. *J. Geophys. Res.*, 93:858–866, 1988.

[24] H.V. Cane. Low frequency maps of the Galaxy. *Proc. Astr. Soc. Aust.*, 2:330–331, 1975.

[25] H.V. Cane and R.G. Stone. Type II solar radio bursts, interplanetary shocks and energetic particle events. *Ap. J.*, 282:339–344, 1984.

[26] H.V. Cane and P.S. Whitham. Observations of the southern sky at five frequencies in the range 2-20 MHz. *Monthly Not. Roy. Astr. Soc.*, 179:21–29, 1977.

[27] T. Carozzi, R. Karlsson, and J. Bergman. Parameters characterizing electromagnetic wave polarization. *Phys. Rev. E.*, 61:2024–2028, 2000.

[28] M.S. Carpenter. *Bibliography of extraterrestrial radio noise*, volume 11-13,15 of *Radio Astr. Rep. Nos.* Cornell University, New York, 1950-1957.

[29] G.P. Chernov. Behaviour of low-frequency waves in coronal magnetic traps. *Soviet Astron.*, 33:649, 1989.

[30] G.P. Chernov et al. New features in type IV solar radio emission: Combined effects of plasma wave resonances and MHD waves. *Astron. Astrophys.*, 334:314–324, 1998.

[31] G. Contopoulos, editor. *Highlights in astronomy.* Reidel Publishing Company, Dordrecht, 1974.

[32] J. Dawson. Radiation from plasmas. In A. Simon and W.B. Thompson, editors, *Advances in plasma physics*, volume 1, pages 1–66, Interscience Publishers, New York, 1968.

[33] C. de Jager and G. de Jonge. Properties of elementary flare bursts. *Sol. Phys.*, 58:127–137, 1978.

[34] J. de la Noë and A. Boischot. The type IIIb burst: A precursor of decametre type III radio-burst. *Astron. Astrophys.*, 20:55–62, 1972.

[35] A.J. Dessler. *Physics of the Jovian magnetosphere.* Cambridge University Press, Cambridge, 1983.

[36] R.H. Dicke and R. Beringer. Microwave radiation from the Sun and the moon. *Ap. J.*, 102:375–376, 1946.

[37] G.A. Dulk et al. The speeds of electrons that excite solar radio bursts of type III. *Astron. Astrophys.*, 173:366–374, 1987.

[38] G.A. Dulk, S. Suzuki, and D.E. Gary. The position and polarization of type V solar bursts. *Astron. Astrophys*, 88:218–229, 1980.

[39] G. Dumas, C. Caroubalos, and J.L. Bougeret. The digital multi-channel radiospectrograph in Nancay. *Sol. Phys.*, 81:383, 1982.

[40] Ø. Elgarøy. *Solar noise storms.* Pergamon Press, Oxford, 1977.

[41] H.I. Ewen and E.M. Purcell. Radiation of hyperfine levels of interstellar hydrogen. *Phys. Rev.*, 83:881, 1951.

[42] D.F. Gray. *The observation and analysis of stellar photospheres.* Cambridge University Press, Cambridge, second edition, 1992.

[43] M. Güdel. Solar radio spikes: Radiation at harmonics s=2-6. *Astron. Astrophys.*, 239:L1–L4, 1990.

[44] M. Güdel and P. Zlobec. Polarization and emission mode for solar radio spikes. *Astron. Astrophys.*, 245:299–309, 1991.

[45] F.T. Haddock. Introduction to radio astronomy. *Proc. IRE*, 46:3–12, 1958.

[46] M. Harwit. *Cosmic discovery: The search, scope and heritage of astronomy.* MIT Press, Cambridge, 1984.

[47] E. Haug. Efficient computation of electron-electron bremsstrahlung emission in a hot thermal plasma. *Astron. Astrophys.*, 218:330–333, 1989.

[48] D.W. Heightman. The UHF: A review of conditions in 1937. *Wireless World*, 42:356–357, 1938.

[49] J.S. Hey. Solar radiation in the 4-6 meter radio wave-length band. *Nature*, 157:47–48, 1946.

[50] J.S. Hey. *The evolution of radio astronomy.* Science History Publications, New York, 1975.

[51] J.S. Hey, S.J. Parsons, and J.W. Phillips. Fluctuations in cosmic radiation at radio frequencies. *Nature*, 158:234, 1946.

[52] A. Hillaris, C.E. Alissandrakis, and L. Vlahos. Dynamics of sub-relativistic electron beams in magnetic traps: A model for solar N-bursts. *Astron. Astrophys.*, 195:301–309, 1988.

[53] S. Hoang et al. Interplanetary fast shock diagnosis with the radio receiver on Ulysses. In E. Marsch and R. Schwenn, editors, *Solar Wind Seven*, pages 465–468, Pergamon Press, Oxford, 1992.

[54] G.D. Holman and M.E. Pesses. Solar type II radio emission and the shock drift acceleration of electrons. *Ap. J.*, 267:837–843, 1983.

[55] H. Isliker et al. A stochastic model for solar type III bursts. *Astron. Astrophys.*, 336:371–380, 1998.

[56] K.G. Jansky. Radio waves from outside the solar system. *Nature*, 132:66, 1933.

[57] D.L. Jones et al. The Astronomical Low-Frequency Array ALFA. In J.A. Zensus, G.B. Taylor, and J.M. Wrobel, editors, *Radio emission from galactic and extragalactic compact sources*, volume 144 of *ASP Conf. Ser.*, pages 393–394, San Francisco, 1988.

[58] S.A. Kaplan and V.N. Tsytovich. *Plasma astrophysics*. Pergamon Press, Oxford, 1973.

[59] M. Karlický, G. Mann, and H. Aurass. Transport of superthermal electrons in coronal loops and U(N)-type solar radio bursts. *Astron. Astrophys.*, 314:303–311, 1996.

[60] A. Klassen et al. On two distinct shocks during the flare of 9 July, 1996. *Sol. Phys.*, 188:141–154, 1999.

[61] A. Klassen et al. Radio evidence on shock wave formation in the solar corona. *Astro. Astrophys.*, 343:287–296, 1999.

[62] A. Klassen et al. Catalogue of the 1997 SOHO-EIT coronal transient waves and associated type II radio burst spectra. *Astron. Astrophys. Suppl. Ser.*, 141:357–369, 2000.

[63] K.-L. Klein et al. X-ray and radio evidence on the origin of a coronal shock wave. *Astron. Astrophys.*, 346:L53–L56, 1999.

[64] B. Kliem, A. Krueger, and R.A. Treumann. Third plasma harmonic radiation in type II bursts. *Sol. Phys.*, 140:149–160, 1992.

[65] N.A. Krall and D.F. Smith. Radiation phenomena in type II solar radio bursts and laboratory shock-wave experiments. *Ap. J.*, 199:500–503, 1975.

[66] V.V. Krasnosel'skikh et al. Fast electron generation in quasiperpendicular shocks and type II solar radio bursts. *Astron. Astrophys.*, 149:323–329, 1985.

[67] R.W. Kreplin et al. High resolution X-ray spectra of solar flares. VII. A long-duration X-ray flare associated with a coronal mass ejection. *Ap. J.*, 292:309–318, 1985.

[68] A. Krüger. *Introduction to solar radio astronomy and radio physics.* Reidel Publishing Company, Dordrecht, 1979.

[69] M.R. Kundu and T.E. Gergely, editors. *Radio physics of the Sun*, volume 86 of *IAU Symp.* Reidel Publishing Company, Dordrecht, 1980.

[70] M. Lampe and K. Papadopoulos. Formation of fast electrons tails in type II solar bursts. *Ap. J.*, 212:886–890, 1977.

[71] O.J. Lodge. *Signalling through space without wires.* The Electrician. London, second edition, 1897.

[72] G. Mann and H.-T. Classen. Electron acceleration to high energies at quasi-parallel shock waves in the solar corona. *Astron. Astrophys.*, 304:576–584, 1995.

[73] G. Mann, T. Classen, and H. Aurass. Characteristics of coronal shock waves and solar type II radio bursts. *Astron. Astrophys.*, 295:775–781, 1995.

[74] G. Mann et al. A heliospheric density model and type III radio bursts. *Astro. Astrophys.*, 348:614–620, 1999.

[75] G. Mann and H. Lühr. Electron acceleration at quasi-parallel shocks in the solar corona and its signature in solar type II radio bursts. *Ap. J. Suppl.*, 90:577–581, 1994.

[76] R. Manning and J. Fainberg. A new method of measuring radio source parameters of a partially polarized distributed source from spacecraft observations. *Space Sci. Inst.*, 5:161–181, 1980.

[77] D.J. McLean and N.R. Labrum. *Solar Radiophysics.* Cambridge University Press, Cambridge, 1985.

[78] D.B. Melrose. *Plasma Astrophysics Vol. 1 and 2.* Gordon and Breach Science Publishers, New York, 1980.

[79] D.B. Melrose. A plasma emission mechanism for type I solar radio emission. *Sol. Phys.*, 67:357–375, 1980.

[80] D.B. Melrose. *Instabilities in space and laboratory plasmas.* Cambridge University Press, Cambridge, 1986.

[81] D. Mihalas. *Stellar atmospheres.* Freeman, San Francisco, second edition, 1978.

[82] J.A. Miller, N. Guessoum, and R. Ramaty. Stochastic Fermi acceleration in solar flares. *Ap. J.*, 361:701–708, 1990.

[83] G.E. Moreton. Hα observations of flare-initiated disturbances with velocities $\sim$1000 km/s. *Astr. J.*, 65:494, 1960.

[84] M. Nakagami and K. Miya. Incident angle of short-waves and high-frequency noise during dellinger effect. *Electrotech. J. Japan*, 3:216, 1939.

[85] B.T. Park, V. Petrosian, and R.A. Schwartz. Stochastic acceleration and photon emission in electron-dominated solar flares. *Ap. J.*, 489:358–366, 1997.

[86] J.L. Pawsey, R. Payne-Scott, and L.L. McCready. Radio-frequency energy from the Sun. *Nature*, 157:158–159, 1946.

[87] R. Payne-Scott, D.E. Yabsley, and J.G. Bolton. Relative times of arrival of solar noise on different frequencies. *Nature*, 160:256–257, 1947.

[88] M. Poquérusse. Relativistic type III solar radio bursts. *Astron. Astrophys.*, 286:611–625, 1994.

[89] E.R. Priest. *Solar Magnetohydrodynamics.* Reidel Publishing Company, Dordrecht, 1982.

[90] A. Raoult, L. Vlahos, and A. Mangeney. An injection model for type III/V bursts in solar flares. *Astron. Astrophys.*, 233:229–234, 1990.

[91] G. Reber. Cosmic static. *Ap. J.*, 100:279–287, 1944.

[92] P.A. Robinson and A.O. Benz. Bidirectional type III solar radio bursts. *Sol. Phys.* in press.

[93] G.B. Rybicki and A.P. Lightman. *Radiative processes in astrophysics.* John Wiley & Sons, New York, 1979.

[94] S.J. Schwartz et al. Observations of short large-amplitude magnetic strutures at a quasi-parallel shock. *J. Geophys. Res.*, 97:4209–4227, 1992.

[95] R. Schwenn and E. Marsch, editors. *Physics of the inner heliosphere 1.* Springer-Verlag, Berlin, 1990.

[96] G.C. Southworth. Microwave radiation from the Sun. *J. Franklin Inst.*, 239:285–297, 1945.

[97] G.C. Southworth. Early history of radio astronomy. *Sci. Monthly*, 82:55–66, 1956.

[98] P.A. Sturrock. Type III solar radio bursts. In W.N. Hess, editor, *Proceedings of the AAS-NASA symposium on the physics of solar flares*, volume 50 of *NASA SP*, page 357, 1964.

[99] P.A. Sturrock et al. Energy release in solar flares. *Sol. Phys.*, 94:341–357, 1984.

[100] M.F. Taylor et al. Analysis of the low-frequency radio noise environment at satellite heights from terrestrial sources. In *AAS 188th Meeting*, volume 28-2 of *Bulletin of the Am. Astron. Soc.*, 1996.

[101] G. Thejappa et al. Evidence for Langmuir envelope solitons in solar type III bursts source regions. *J. Geophys. Res.*, 104:28279, 1999.

[102] I.N. Toptygin. Acceleration of particles by shocks in a cosmic plasma. *Space Sci. Rev.*, 26:157–213, 1980.

[103] V.N. Tsytovich. *Nonlinear effects in plasmas.* Plenum Press, New York, 1970.

[104] L. Vlahos and A. Raoult. Beam fragmentation and type III bursts. *Astron. Astrophys.*, 296:844–849, 1995.

[105] W.J. Wagner and R.M. MacQueen. The excitation of type II radio bursts in the corona. *Astron. Astrophys.*, 120:136–138, 1983.

[106] R.R. Weber, J.K. Alexander, and R.G. Stone. The Radio Astronomy Explorer satellite, a low frequency observatory. *Radio Science*, 6:1085–1098, 1971.

[107] K.W. Weiler, editor. *Radio astronomy from space: Proc. of a workshop held at the the National Radio Astronomy Observatory Green Bank, West Virginia 30 September to 2 October 1986.* NRAO, 1987.

[108] K.W. Weiler, B.K. Dennison, and K.J. Johnson. Radio astronomy looks to space. *Astronomy*, 16-5:18, 1988.

[109] K.W. Weiler et al. A low frequency radio array for space. *Astron. Astrophys.*, 195:372–379, 1988.

[110] K.W. Weiler and N.E. Nassim, editors. *Low frequency astrophysics from space: Proc. of an international workshop held in Crystal City, Virginia on 8 and 9 January 1990.* Springer-Verlag, Berlin, 1990.

[111] K.W. Weiler and N.E. Nassim. Low frequency radio astronomy from Earth orbit. In Y. Kondo, editor, *Observatories in Earth orbit and beyond*, page 508, Kluwer Publishers, Dordrecht, 1990.

[112] J.P. Wild. Observations of the spectrum of high-intensity solar radiation at metre wavelengths - III. Isolated bursts. *Aust. J. Sci. Res.*, Ser. A., 3:541, 1950.

[113] R.M. Winglee and G.A. Dulk. The electron-cyclotron maser instability as a source of plasma radiation. *Ap. J.*, 307:808–819, 1986.

[114] V.V. Zaitsev. Stimulated plasma-wave scattering during generation of high-frequency solar type III radio bursts. *Pis'ma v Astron. Zh.*, 1:28–33, 1975. In Russian.

[115] V.V. Zaitsev. Theory of solar II and III radio bursts. *Radiofizika*, 20:1379–1398, 1977. In Russian.

[116] V.V. Zheleznyakov. *Radio emission of the Sun and the planets.* Pergamon Press, Oxford, 1970.

[117] V.V. Zheleznyakov. *Electromagnetic waves in space plasma.* Izdatel'stvo Nauka, Moscow, 1977. In Russian.

[118] V.V. Zheleznyakov. *Radiation in astrophysical plasmas.* Kluwer Academic Publishers, Dordrecht, 1996.

[119] V.V. Zheleznyakov and E.Y. Zlotnik. On the third harmonic in solar radio bursts. *Sol. Phys.*, 36:443–449, 1974.

[120] E.Y. Zlotnik et al. Third harmonic plasma emission in solar type II radio bursts. *Astron. Astrophys.*, 331:1087–1098, 1998.